STATISTICS, OPTIMIZATION AND INFORMATION COMPUTING
Stat., Optim. Inf. Comput., Vol. **x**, Month 202x, pp 0–38.
Published online in International Academic Press (www.IAPress.org)

Pythagorean Neutrosophic Framework and Its Application to Correlation-Based Threat Identification

Jamil J. Hamja [1], Walid Abdelfattah [2,*], Aqeedat Hussain [3], Arif Mehmood[3], Sisteta U. Kamdon[4], Noor-Han N. Ulal[5], Al-jayson U. Abubakar[6], Cris L. Armada[7,8]

[1]*Department of Mathematics, College of Mathematical Sciences, Mindanao State University-Tawi-Tawi College of Technology and Oceanography, 7500 Philippines*
[2]*Humanities and Social Research Center, Northern Border University, Arar, Saudi Arabia*
[3]*Department of Mathematics, Institute of Numerical Sciences, Gomal University, Dera Ismail Khan 29050, KPK, Pakistan*
[4]*Department of Mathematics, College of Mathematical Sciences, Mindanao State University Tawi-Tawi College of Technology and Oceanography*
[5]*Human Resource Development Office, MSU-TCTO, Sanga-Sanga, Bongao, Tawi-Tawi, 7500, Philippines*
[6]*Integrated Laboratory School, College of Education, Mindanao State University Tawi-Tawi College of Technology and Oceanography-Tawi-Tawi, 7500 Philippines*
[7]*Vietnam National University Ho Chi Minh City, Linh Trung Ward, Thu Duc City, Ho Chi Minh City, Vietnam*
[8]*Department of Applied Mathematics, Faculty of Applied Science, Ho Chi Minh City University of Technology (HCMUT), 268 Ly Thuong Kiet, Ward 14, District 10, Ho Chi Minh City, Vietnam*

Abstract In intelligence analysis, surveillance systems, and threat assessments, usual models that rely on discrete mathematics often do not capture the ambiguity in the information well. Uncertainty, incompleteness, and inconsistency are common in intelligence analysis, surveillance systems, and threat assessment, where traditional mathematical models are often unable to adequately describe the ambiguity in the information. In this paper, a Pythagorean neutrosophic framework, called Pythagorean Neutrosophic Framework (PNF), is developed for threat identification in uncertain environment, based on the correlation features. This proposed framework will integrate the expressive power of Pythagorean neutrosophic sets with a new correlation measure that will consider all three degrees of membership: the truth-membership, indeterminacy-membership and falsity-membership degree and will satisfy the Pythagorean constraint. Complement, union and intersection are introduced on Pythagorean neutrosophic sets and a normalized correlation coefficient is introduced that is bounded, symmetric, and identity. The suggested correlation value is then used to correlate observed behavioural indicators to threat categories that have been pre-defined. A case study of a real threat identification scenario shows that the framework is applicable in practice through the use of behavioural characteristics like thermal signature, pattern of movement, weapon handling and communication activity. The values of correlation obtained give a good separation of the various behavioural profiles and are close to the correct classification of the most likely threat category for each target for uncertain information. A series of visualization and analytical methods such as heatmaps, normalized heatmaps, two-dimensional and three-dimensional bar graphs, surface plots, spline interpolation, principal component analysis (PCA), t-distributed stochastic neighbour embedding (t-SNE) and parallel coordinate plots are used to further validate the proposed methodology. The stability, interpretability and discriminatory power of the proposed correlation measure is confirmed by the graphical analysis. The proposed Pythagorean neutrosophic framework is an interpretable mathematical model that manages uncertainty-aware threat identification, and is a potential alternative to the classical similarity measures in the field of security intelligence, decision support systems and other applications using incomplete and conflicting information.

Keywords Pythagorean Neutrosophic Sets; Neutrosophic Correlation Measure; Behavioural Similarity; Threat Classification; Uncertain Information Modelling; Target Behaviour Mapping.

AMS 2010 subject classifications 68M10

DOI: 10.19139/soic-2310-5070-4383

*Correspondence to: Walid Abdelfattah (Email: walid.abdelfattah@nbu.edu.sa). Humanities and Social Research Center, Northern Border University, Arar, Saudi Arabia.

ISSN 2310-5070 (online) ISSN 2311-004X (print)

1. Introduction

Complex challenges in the real world Uncertainty, imprecision, and incomplete truth are common issues that hamper decision-making and pattern recognition problems. This vast gradation cannot be adequately described by the traditional binary logic, which is predicated on the elements being either fully a part of a set or not. Zadeh [1] introduced the idea of fuzzy sets, which marked the beginning of a paradigm shift. By providing the concepts with their degrees of membership, this structure revolutionized the description of amorphous knowledge and provided a mathematical language of non-crunchy concepts. Since then, the field's development has split into a number of powerful generalizations that each seek to address certain types of uncertainty. The Turksen [2] developed the idea of interval-valued fuzzy sets to address the imprecision of specifying the membership degree per se. Simultaneously, Atanassov [3] presented an even more profound generalization using intuitionistic fuzzy sets (IFS), which explicitly convey reluctance by describing each object in terms of both a membership degree and a non-membership degree. Atanassov and Gargov [4] expanded this further to reflect even greater uncertainty in interval-valued intuitionistic fuzzy sets. Strong comparison and analysis measures are essential for the efficient application of these set theories, and Liu has made substantial progress in this area with his work on entropy, distance, and similarity measurements of fuzzy sets [5].
Some of the most significant literature, such as the article by Pedrycz and Gomide [6] and the mathematical operators underlying fuzzy logic, particularly the triangular norms, formalized by Klement, Mesiar, and Pap [8], covered in detail the pedagogical and applied foundations of the concepts. An overview of the entire field has been given by Zimmermann [9]. Smarandache developed the neutrosophic [7] and neutrosophic set [11] models in an effort to provide a more comprehensive representation of truth, indeterminacy, and falsity separately. It is a significant extension of the intuitionistic fuzzy set, a conceptual leap that Wang et al. later refined for computational application in interval neutrosophic sets [12]. The application of these sophisticated set theories to key issues demonstrates their utility. The development of new IFS similarity measures by Li and Cheng [10]and Lp metric measures by Hung and Yang [13] has proven beneficial in pattern identification. Cheng and Guo have developed novel techniques for picture segmentation [15] and thresholding [14] as a result of the neutrosophic model's exceptional success in image processing. Additionally, Ye has used these ideas in the context of automated decision-making to create complex multi-criteria decision-making procedures on interval-valued intuitionistic fuzzy settings [16] and group decisions based on intuitionistic trapezoidal fuzzy numbers [17].

1.1. Literature Review

The evolution of set theory in handling uncertainty has progressed from warehouses of simple fuzzy sets to more sophisticated structures that can handle the intricacy of real-world data. The constraint that the degree of membership and non-membership should add to one or less limits the enormous improvements that Intuitionistic Fuzzy Sets (IFS) [3] and their neutrosophic generalizations [11, 12] offered by incorporating hesitation and indeterminacy. The concept of Pythagorean Fuzzy Sets (PFS) was introduced to reflect an even wider range of uncertainty, particularly when the decision-makers supply complex judgments that are not restricted by this criterion. This criterion can be loosened by using a Pythagorean fuzzy set, which merely requires that the square sum of the membership and non-membership degrees be less than or equal to one (i.e., $\mu_2 + \nu_2$). As a result, it can issue membership grades in a wider and more flexible manner. The Pythagorean framework and the neutrosophic philosophy were combined to create the powerful hybrid structure known as the Pythagorean Neutrosophic Set (PNS). A PNS is a combination of the Pythagorean condition, which is subject to $T_2 + F_2 = 1$, and the indeterminacy (I), falsity (F) membership structure of neutrosophic sets. This combination, as is discussed in [18], creates a powerful representation of knowledge in which the measures of neutrality, opposition, and support are not only independent but also more ambiguous and uncertain due to the Pythagorean restriction. The theoretical foundation of PNS has been strengthened by the creation of the required operational regulations and aggregation operators. In this regard, [21] made a significant contribution by developing new operating rules that offer flexibility and generalizability utilizing the Dombi t-norm and t-conorm. Additionally, they expanded a collection of aggregation operators, such as the Pythagorean neutrosophic Dombi weighted arithmetic and geometric operators, which are crucial for synthesizing data from several sources in a multi-criteria decision-making (MCDM) situation.

During the aggregation process, these operators effectively preserve the unique characteristics of Pythagorean neutrosophic information. The Pythagorean Neutrosophic Sets have been shown to be practical in a variety of applications, the most important of which is in the area of important decision-making. [22] developed an MCDM model specifically to choose sustainable suppliers in a supply chain, a problem rife with social, environmental, and economic uncertainty. In order to address the ambiguous and frequently contradictory character of sustainability measurements, they employed a long-run TOPSIS (Technique for Order Preference by Similarity to Ideal Solution) methodology in the Pythagorean neutrosophic environment. This application demonstrates the suitability of PNS for real-world problems where the application of expertise is nuanced and ambiguous. PNS is discovering its use in addition to choosing vendors. It is utilized in fields such as financial portfolio selection, where market forecasts are ambiguous, and medical diagnosis, where symptoms and their correlation with illnesses have significant levels of ambiguity and conflicting information. PNS's enhanced usefulness in pattern recognition and clustering analysis is also a result of the development of new distance measures, similarity measures, and correlation coefficients. The evolution of uncertainty mathematical models has significantly progressed from classical fuzzy sets to more sophisticated fuzzy sets that can reflect lower levels of indeterminacy, such as neutrosophic and plithogenic sets. In order to solve nonlinear equations that are formulated in these generalized frameworks, this theoretical expansion necessitates the concurrent development of computation procedures. This dual focus is demonstrated by recent research that creates consistent formalisms of type-n extensions of fuzzy, neutrosophic, and plithogenic offsets, which are necessary for applied studies to have a theoretical foundation [23]. Subsequent research has developed numerical structures for certain types of issues, including addressing neutrosophic difficulties, based on such frameworks. Weak fuzzy analysis [24], derivative problems based on Newton, complex differential equations [25], and the creation of practical methods to solve weak fuzzy complex Diophantine equations [26]. The application of numerical methods to partial differential equations is also represented in earlier contributions. when circumstances become hazy, as in the case of the complex bounds of the fuzzy heat equation [27]. The publications in [23]-[27] collectively provide a clear research path that emphasizes the current trend of creating increasingly complicated uncertainty-driven systems through effort, beginning with theoretical, conceptual unity and moving toward applied, algorithmic solvability and computationally manageable.

The study of correlation functions of non-stationary fields with a zero-spectrum yielded significant theoretical advancements in the science of stochastic processes [28]. Subsequently, the structure of the operator set and its spectra in a Hilbert space were better understood, and two-dimensional model representations of commuting operators were created [29]. The development of model representations for non-self-adjoint operators with indefinitely dimensional imaginary parts furthered this line of inquiry and significantly aided in the spectral analysis of linear operators [30]. Additionally, the theory of operator systems and their applications was expanded by the proposal of triangular models of commutative systems of linear operators approaching unitary operators [31]. A spline-based numerical solution for linear two-point boundary value problems was developed as a result of further research, and it was more computationally efficient and accurate than traditional approaches [32]. Additionally, the Gierer-Meinhardt reaction-diffusion system's finite-time stability and control were examined, providing a useful theoretical understanding of how nonlinear dynamical systems with partial differential equations behave [33]. New numerical radius inequalities in functional analysis have led to improved classical results and tighter bounds for bounded linear operators [34]. A powerful mathematical tool for handling uncertainty in algebraic systems and decision-making applications is the mathematical framework of 2-fold fuzzy n-refined neutrosophic algebraic structures (n=2,3), which was expanded from neutrosophic algebraic structures and developed in a new manner more recently [35].

1.2. Motivation and Significance

Modern analytical systems, especially those in high-stakes settings like security, surveillance, and real-time threat assessment, are plagued by the issue of ambiguous, incomplete, and contradictory data. When data contains both degrees of truth and falsehood as well as indeterminacy, the previous crisp and fuzzy models struggle to describe the situation. The employment of Pythagorean Neutrosophic Sets (PNS), which provide a mathematically uniform model of uncertainty to membership, indeterminacy, and non-membership components under Pythagorean constraints, is justified by this gap. In order to manage uncertain information rigorously rather than heuristically, the framework portrays the uncertain information as codified acting according to the fundamental set operations, such as complement, union, and intersection. The need to compare the ambiguous behavioral patterns numerically is another factor. In order to address this, the suggested neutrosophic correlation measure uses the squared truth, indeterminacy, and falsity values to gauge how similar two neutrosophic profiles are. It is a powerful analytical tool that serves as the theoretical foundation for additional behavioral interpretation because it is symmetric and bounded. The foundation is particularly crucial for converting intricate and multi-source surveillance signals, such motion dynamics, communication traces, thermal signatures, or weapon-handling behaviors, into organized metrics that may be used to inform operational choices. In the context of the threat-identification scenario that is applied to the real world in this study, the significance of the framework may be clearly appreciated. Target T_2 shows a good congruence with low-threat behavior (0.896), but T_1 presents a strong similarity to indicators that are militant (0.744). The mixed and moderate associations of T_3 indicate an uncertain profile. These results show that the neutrosophic correlation operator can effectively measure behavioral tendencies, minimize uncertainty, and present modest but operationally significant differences between targets. Additionally, the hybrid aspect-method explanation proves the greater meaning of the approach. Aspect-wise, the model systematically distinguishes between high- and low-risk behavioral profiles (and as an interim group) the T_2 and T_3, and the T_1 as an anomalous entity. The analytical method-wise, the correlation structure is consistent over a variety of the analysis methods, such as Heatmaps, PCA embeddings, clustering results, and smooth surface representation, highlighting the stability and strength of the method. Overall, the work's rationale is to address the problem of making decisions in the face of uncertainty.

1.3. Research Novelty

This study offers some novel theoretical and practical insights that can further the use of neutrosophic theory in danger assessment and behavioral modeling. It proposes a new Pythagorean neutrosophic correlation model that incorporates squared membership, indeterminacy, and non-membership elements on Pythagorean constraints. It also offers a more sophisticated similarity measure that can identify minute behavioral differences that are not picked up by coarser fuzzy or neutrosophic measures. The second feature is that the surveillance evidence is more realistic and multi-layered because two related structures the target-behavior relation and the behavior-threat relation are integrated into a single correlation chain.

The work also presents a hybrid aspect-method interpretation in which the method-based analysis demonstrates computational stability on Heatmaps, PCA embeddings, spline curves, clustering outputs, and 3D surfaces, while the aspect-based analysis finds behavioral groupings, high-risk anomalies, and low-risk clusters. In correlation-based neutrosophic models, this two-sided viewpoint provides strength where none had been demonstrated. The other noteworthy contribution is the first application of Pythagorean neutrosophic correlation to a real threat-identification problem, using security intelligence of multi-source behavioral data, such as thermal patterns, movement dynamics, and communication signals, rather than standard medical or diagnostic data. Because this architecture produces interpretable correlation values and behavioral signatures that are visually consistent across analysis levels, it is also a mathematically consistent and interpretable alternative to black-box AI systems. Finally, the model reveals important associations such as the militant character of T_1 (0.744), the ambiguous profile of T_3, and the high low-threat alignment of T_2 (0.896), offering new insights into behavioral similarity and differentiation under ambiguous information. These results demonstrate the model's ability to identify patterns that would otherwise be hidden within inconsistent, noisy, or incomplete data.

1.4. Research Contribution

The main results of this study are as follows:

1. A mathematical model of Pythagorean neutrosophic sets which is a comprehensive mathematical structure is built to model uncertainty that contains truth, indeterminacy and falsity under Pythagorean constraint.
2. A new correlation coefficient is suggested to measure the similarity of Pythagorean neutrosophic sets and keep some important features of it such as symmetry, boundedness and identity.
3. A detailed theoretical examination is performed in order to prove mathematically the validity of the proposed correlation measure.

4. In order to reflect the correlation between the behavioural indicators and the categories of threats, a practical threat identification framework is introduced, based on neutrosophic correlation analysis.
5. To validate the efficiency of the proposed model, extensive graphical analyses, such as heatmaps, normalized heatmaps, bar graphs, 3D visualization, spline plotting, principal component analysis, t-SNE and parallel coordinate plots are used.
6. An interpretable mathematical alternative to black-box machine learning approaches to uncertainty-aware behavioural analysis is proposed in the framework. The methodology can be applied to many fields such as medical diagnosis, cybersecurity, pattern recognition, intelligent surveillance, multi-criteria decision making and risk assessment.

1.5. Organization of the Paper

The rest of this paper is organized as follows:
The theoretical foundation of the proposed framework is discussed in terms of the basic concepts of intuitionistic fuzzy sets, neutrosophic sets and Pythagorean neutrosophic sets in Section 2. In Section 3, the proposed Pythagorean neutrosophic correlation measure, its mathematical properties and proofs are introduced. The methodology and visualization techniques employed during performance evaluation are included in Section 4. The viability of the proposed framework is shown in Section 5 by a problem of threat identification that is inspired by a real-world scenario. The computational results are discussed in Section 6 with the aid of different visualization techniques. Finally, Section 7 summarizes the findings of the major work, discusses the limitations of the proposed work and future research directions.

2. Preliminaries

This section presents the foundational concepts required for the subsequent sections.

Definition 2.1
[3] If $\mathcal{E}$ be a universe. An intuitionistic fuzzy set $\mathcal{A}$ on $\mathcal{E}$ can be defined as follows:

$$\mathcal{A} = \{\langle x, \mu_{\mathcal{A}}(x) + \vartheta_{\mathcal{A}}(x)\rangle : x \in \mathcal{X}\}$$

where, $\mu_{\mathcal{A}}(x) : \mathcal{E} \to [0,1]$ and , $\vartheta_{\mathcal{A}}(x) : \mathcal{E} \to [0,1]$ denote respectively the degree of membership and degree of non-membership of each element $x \in \mathcal{X}$ to the set P, and $0 \leq (\mu_{\mathcal{A}}(x))^2 + (\vartheta_{\mathcal{A}}(x))^2 \leq 1$ for each $x \in \mathcal{X}$.

Definition 2.2
[19] Suppose $\mathcal{X}$ be a non-empty set. A pythagorean fuzzy set $\mathcal{A}$ on $\mathcal{X}$ is an object of the form:

$$\mathcal{A} = \{\langle x, \mu_{\mathcal{A}}(x) + \vartheta_{\mathcal{A}}(x)\rangle : x \in \mathcal{X}\}$$

where the function, $\mu_{\mathcal{A}}(x) : \mathcal{X} \to [0,1]$ and , $\vartheta_{\mathcal{A}}(x) : \mathcal{X} \to [0,1]$ and $0 \leq (\mu_{\mathcal{A}}(x))^2 + (\vartheta_{\mathcal{A}}(x))^2 \leq 1$ and $(\zeta_{\mathcal{A}}(x))^2 \leq 1$. Thus $0 \leq (\mu_{\mathcal{A}}(x))^2 + (\zeta_{\mathcal{A}}(x))^2 + (\vartheta_{\mathcal{A}}(x))^2 \leq 2$ for each $x \in \mathcal{X}$. $\mu_{\mathcal{A}}(x)$ is the degree of membership, $\zeta_{\mathcal{A}}(x)$ is the degree of indeterminacy and $\vartheta_{\mathcal{A}}(x)$ is the degree of non-membership. Here $\mu_{\mathcal{A}}(x)$ and $\vartheta_{\mathcal{A}}(x)$ are dependent components and $\zeta_{\mathcal{A}}(x)$ is an independent component.

Definition 2.3
[20] Consider $\mathcal{X}$ be a non-empty set. A neutrosophic set $\mathcal{A}$ on $\mathcal{X}$ is an object of the form:

$$\mathcal{A} = \{\langle x, \mu_{\mathcal{A}}(x) + \zeta_{\mathcal{A}}(x) + \vartheta_{\mathcal{A}}(x)\rangle : x \in \mathcal{X}\}$$

where, $\mu_{\mathcal{A}}(x), \zeta_{\mathcal{A}}(x), \vartheta_{\mathcal{A}}(x) \in [0,1]$ and $0 \leq (\mu_{\mathcal{A}}(x)) + (\zeta_{\mathcal{A}}(x)) + (\vartheta_{\mathcal{A}}(x)) \leq 3$ for each $x \in \mathcal{X}$. $\mu_{\mathcal{A}}(x)$ is the degree of membership, $\zeta_{\mathcal{A}}(x)$ is the degree of indeterminacy and $\vartheta_{\mathcal{A}}(x)$ is the degree of non-membership. Here $\mu_{\mathcal{A}}(x)$ and $\vartheta_{\mathcal{A}}(x)$ are dependent components and $\zeta_{\mathcal{A}}(x)$ is an independent component.

Definition 2.4
[20] Let $\mathcal{X}$ be a space of points (objects), with a generic element in $\mathcal{X}$ denoted by x. For SVNS $\mathcal{A}$ and $\mathcal{B}$. $\mathcal{A} \subseteq \mathcal{B}$ if and only if $T_{\mathcal{A}}(x) \leq T_{\mathcal{B}}(x)$, $I_{\mathcal{A}}(x) \geq I_{\mathcal{B}}(x)$, $F_{\mathcal{A}}(x) \geq F_{\mathcal{B}}(x)$ for any $x \in \mathcal{X}$. Also $\mathcal{A} = \mathcal{B}$ if and only if $\mathcal{A} \subseteq \mathcal{B}$ and $\mathcal{B} \subseteq \mathcal{A}$.

Definition 2.5
[20] If $\mathcal{X}$ be a nonempty set. A neutrosophic set $\mathcal{A}$ and $\mathcal{B}$ of the form

$$\mathcal{A} = \{\langle x, \mu_{\mathcal{A}}(x) + \zeta_{\mathcal{A}}(x) + \vartheta_{\mathcal{A}}(x)\rangle : x \in \mathcal{X}\}$$

and

$$\mathcal{B} = \{\langle x, \mu_{\mathcal{B}}(x) + \zeta_{\mathcal{B}}(x) + \vartheta_{\mathcal{B}}(x)\rangle : x \in \mathcal{X}\}$$

Then, 1.

$$\mathcal{A}^c = \{\langle x, \mu_{\mathcal{A}}(x) + 1 - \zeta_{\mathcal{A}}(x) + \vartheta_{\mathcal{A}}(x)\rangle : x \in \mathcal{X}\}.$$

2.

$$\mathcal{A} \cup \mathcal{B} = \{\langle x, \max(\mu_{\mathcal{A}}(x), \mu_{\mathcal{B}}(x)) + \min(\zeta_{\mathcal{A}}(x), \zeta_{\mathcal{B}}(x)) + \min(\vartheta_{\mathcal{A}}(x), \vartheta_{\mathcal{B}}(x))\rangle : x \in \mathcal{X}\}.$$

3.

$$\mathcal{A} \cap \mathcal{B} = \{\langle x, \min(\mu_{\mathcal{A}}(x), \mu_{\mathcal{B}}(x)) + \min(\zeta_{\mathcal{A}}(x), \zeta_{\mathcal{B}}(x)) + \max(\vartheta_{\mathcal{A}}(x), \vartheta_{\mathcal{B}}(x))\rangle : x \in \mathcal{X}\}.$$

4. $\mathcal{A} \subseteq \mathcal{B}$ if and only if $\mu_{\mathcal{A}}(x) \leq \mu_{\mathcal{B}}(x)$, $\zeta_{\mathcal{A}}(x) \leq \zeta_{\mathcal{B}}(x)$, $\vartheta_{\mathcal{A}}(x) \geq \vartheta_{\mathcal{B}}(x)$.

3. Pythagorean Neutrosophic sets and the Proposed Correlation Measure

Definition 3.1
Let $\mathcal{X}$ be a non-empty set. A pythagorean neutrosophic set $\mathcal{A}$ on $\mathcal{X}$ is an object of the form:

$$\mathcal{A} = \{\langle x, \mu_{\mathcal{A}}(x) + \zeta_{\mathcal{A}}(x) + \vartheta_{\mathcal{A}}(x)\rangle : x \in \mathcal{X}\}$$

where, $\mu_{\mathcal{A}}(x), \zeta_{\mathcal{A}}(x), \vartheta_{\mathcal{A}}(x) \in [0, 1]$ and $0 \leq (\mu_{\mathcal{A}}(x))^2 + (\vartheta_{\mathcal{A}}(x))^2 \leq 1$ and $(\zeta_{\mathcal{A}}(x))^2 \leq 1$. Thus $0 \leq (\mu_{\mathcal{A}}(x))^2 + (\zeta_{\mathcal{A}}(x))^2 + (\vartheta_{\mathcal{A}}(x))^2 \leq 2$ for each $x \in \mathcal{X}$. $\mu_{\mathcal{A}}(x)$ is the degree of membership, $\zeta_{\mathcal{A}}(x)$ is the degree of indeterminacy and $\vartheta_{\mathcal{A}}(x)$ is the degree of non-membership. Here $\mu_{\mathcal{A}}(x)$ and $\vartheta_{\mathcal{A}}(x)$ are dependent components and $\zeta_{\mathcal{A}}(x)$ is an independent component.
The flexibility of the independent indeterminacy degree makes PNSs very useful to represent incomplete, inconsistent and uncertain information, which is not found in the intuitionistic fuzzy and Pythagorean fuzzy models.

Remark 3.1
The inclusion of the independent indeterminacy degree provides greater flexibility than intuitionistic fuzzy and Pythagorean fuzzy models, making PNSs particularly suitable for representing incomplete, inconsistent, and uncertain information

Definition 3.2
Suppose that $\mathcal{X}$ be a nonempty set and I the unit interval [0,1]. Pythagorean neutrosophic set $\mathcal{A}$ and $\mathcal{B}$ of the form

$$\mathcal{A} = \{\langle x, \mu_{\mathcal{A}}(x) + \zeta_{\mathcal{A}}(x) + \vartheta_{\mathcal{A}}(x)\rangle : x \in \mathcal{X}\}$$

and

$$\mathcal{B} = \{\langle x, \mu_{\mathcal{B}}(x) + \zeta_{\mathcal{B}}(x) + \vartheta_{\mathcal{B}}(x)\rangle : x \in \mathcal{X}\}$$

Then, 1.

$$\mathcal{A}^c = \{\langle x, \mu_{\mathcal{A}}(x) + 1 - \zeta_{\mathcal{A}}(x) + \vartheta_{\mathcal{A}}(x)\rangle : x \in \mathcal{X}\}.$$

2. $\mathcal{A} \subseteq \mathcal{B}$ if and only if $\mu_{\mathcal{A}}(x) \leq \mu_{\mathcal{B}}(x)$, $\zeta_{\mathcal{A}}(x) \leq \zeta_{\mathcal{B}}(x)$, $\vartheta_{\mathcal{A}}(x) \geq \vartheta_{\mathcal{B}}(x)$.

3.
$$\mathcal{A}\cup\mathcal{B}=\{\langle x,\max(\mu_{\mathcal{A}}(x),\mu_{\mathcal{B}}(x))+\max(\zeta_{\mathcal{A}}(x),\zeta_{\mathcal{B}}(x))+\min(\vartheta_{\mathcal{A}}(x),\vartheta_{\mathcal{B}}(x))\rangle : x\in\mathcal{X}\}.$$
4.
$$\mathcal{A}\cap\mathcal{B}=\{\langle x,\min(\mu_{\mathcal{A}}(x),\mu_{\mathcal{B}}(x))+\min(\zeta_{\mathcal{A}}(x),\zeta_{\mathcal{B}}(x))+\max(\vartheta_{\mathcal{A}}(x),\vartheta_{\mathcal{B}}(x))\rangle : x\in\mathcal{X}\}.$$

Definition 3.3
If $\mathcal{X}$ be a nonempty set. A Pythagorean neutrosophic set with $\mu_{\mathcal{A}}(x)$ and $\vartheta_{\mathcal{A}}(x)$ are dependent components [PNS] $\mathcal{A}$ and $\mathcal{B}$ of the form
$$\mathcal{A}=\{\langle x,\mu_{\mathcal{A}}(x)+\zeta_{\mathcal{A}}(x)+\vartheta_{\mathcal{A}}(x)\rangle : x\in\mathcal{X}\}$$
and
$$\mathcal{B}=\{\langle x,\mu_{\mathcal{B}}(x)+\zeta_{\mathcal{B}}(x)+\vartheta_{\mathcal{B}}(x)\rangle : x\in\mathcal{X}\}$$
then the correlation coefficient of $\mathcal{A}$ and $\mathcal{B}$
$$\rho(\mathcal{A},\mathcal{B})=\frac{C(\mathcal{A},\mathcal{B})}{\sqrt{C(\mathcal{A},\mathcal{A})\times C(\mathcal{B},\mathcal{B})}}$$
$$C(\mathcal{A},\mathcal{B})=\sum_{i=1}^{n}\{(\mu_{\mathcal{A}}(x_i))^2(\mu_{\mathcal{B}}(x_i))^2+(\zeta_{\mathcal{A}}(x_i))^2(\zeta_{\mathcal{B}}(x_i))^2+(\vartheta_{\mathcal{A}}(x_i))^2(\vartheta_{\mathcal{B}}(x_i))^2\}$$
$$C(\mathcal{A},\mathcal{A})=\sum_{i=1}^{n}\{(\mu_{\mathcal{A}}(x_i))^2(\mu_{\mathcal{A}}(x_i))^2+(\zeta_{\mathcal{A}}(x_i))^2(\zeta_{\mathcal{A}}(x_i))^2+(\vartheta_{\mathcal{A}}(x_i))^2(\vartheta_{\mathcal{A}}(x_i))^2\}$$
and
$$C(\mathcal{B},\mathcal{B})=\sum_{i=1}^{n}\{(\mu_{\mathcal{B}}(x_i))^2(\mu_{\mathcal{B}}(x_i))^2+(\zeta_{\mathcal{B}}(x_i))^2(\zeta_{\mathcal{B}}(x_i))^2+(\vartheta_{\mathcal{B}}(x_i))^2(\vartheta_{\mathcal{B}}(x_i))^2\}$$

3.1. Proposed Correlation Measure

It is provided in this form to ensure that the correlation value is always within the range of 0 to 1.
The proposed measure is based on three independent sources of information for similarity:
- Truth-membership similarity
- Indeterminacy similarity
- Falsity-membership similarity

Therefore, the measure is able to distinguish the uncertain behavioural profiles better than the traditional fuzzy similarity measures.

Proposition 1
The defined correlation measure between PNS $\mathcal{A}$ and $\mathcal{B}$ satisfies the following properties:

1. $0\leq\rho(\mathcal{A},\mathcal{B})\leq 1$.
2. $\rho(\mathcal{A},\mathcal{B})=1$ iff $\mathcal{A}=\mathcal{B}$.
3. $\rho(\mathcal{A},\mathcal{B})=\rho(\mathcal{B},\mathcal{A})$.

Proof

1. $0\leq S(\mathcal{A},\mathcal{B})\leq 1$. As μ, ζ and ϑ membership functions of the PNS lies between 0 and 1, $\rho(\mathcal{A},\mathcal{B})$ is also lies between 0 and 1.
   We will prove
$$C(\mathcal{A},\mathcal{B})=\sum_{i=1}^{n}\{(\mu_{\mathcal{A}}(x_i))^2(\mu_{\mathcal{B}}(x_i))^2+(\zeta_{\mathcal{A}}(x_i))^2(\zeta_{\mathcal{B}}(x_i))^2+(\vartheta_{\mathcal{A}}(x_i))^2(\vartheta_{\mathcal{B}}(x_i))^2\}$$

$$= \{(\mu_{\mathcal{A}}(x_1))^2(\mu_{\mathcal{B}}(x_1))^2 + (\zeta_{\mathcal{A}}(x_1))^2(\zeta_{\mathcal{B}}(x_1))^2 + (\vartheta_{\mathcal{A}}(x_1))^2(\vartheta_{\mathcal{B}}(x_1))^2\}$$
$$= ((\mu_{\mathcal{A}}(x_1))^2(\mu_{\mathcal{B}}(x_1))^2 + (\vartheta_{\mathcal{A}}(x_1))^2(\vartheta_{\mathcal{B}}(x_1))^2) + (((\zeta_{\mathcal{A}}(x_1))^2(\zeta_{\mathcal{B}}(x_1))^2) + ...+$$
$$\{(\mu_{\mathcal{A}}(x_n))^2(\mu_{\mathcal{B}}(x_n))^2 + (\zeta_{\mathcal{A}}(x_n))^2(\zeta_{\mathcal{B}}(x_n))^2 + (\vartheta_{\mathcal{A}}(x_n))^2(\vartheta_{\mathcal{B}}(x_n))^2\}$$

By Cauchy-Schwarz inequality, $(x_1y_1 + x_2y_2 + ... + x_ny_n)^2 \leq (x_1^2 + x_2^2 + ... + x_n^2).(y_1^2 + y_2^2 + ... + y_n^2)$ where $(x_1^2 + x_2^2 + ... + x_n^2) \in R^n$ and $(y_1^2 + y_2^2 + ... + y_n^2) \in R^n$

$$C(\mathcal{A},\mathcal{B})^2 = ((\mu_{\mathcal{A}}(x_1))^4 + (\zeta_{\mathcal{A}}(x_1))^4 + (\vartheta_{\mathcal{A}}(x_1))^4) + ((\mu_{\mathcal{A}}(x_2))^4 + (\zeta_{\mathcal{A}}(x_2))^4 + (\vartheta_{\mathcal{A}}(x_2))^4) + ...+$$
$$((\mu_{\mathcal{A}}(x_n))^4 + (\zeta_{\mathcal{A}}(x_n))^4 + (\vartheta_{\mathcal{A}}(x_n))^4)\times$$
$$((\mu_{\mathcal{B}}(x_1))^4 + (\zeta_{\mathcal{B}}(x_1))^4 + (\vartheta_{\mathcal{B}}(x_1))^4) + ((\mu_{\mathcal{B}}(x_2))^4 + (\zeta_{\mathcal{B}}(x_2))^4 + (\vartheta_{\mathcal{B}}(x_2))^4) + ...+$$
$$(\mu_{\mathcal{B}}(x_n))^4 + (\zeta_{\mathcal{B}}(x_n))^4 + (\vartheta_{\mathcal{B}}(x_n))^4)$$
$$((\mu_{\mathcal{A}}(x_1))^4(\mu_{\mathcal{A}}(x_1))^4 + (\zeta_{\mathcal{A}}(x_1))^4(\zeta_{\mathcal{A}}(x_1))^4 + (\vartheta_{\mathcal{A}}(x_1))^4(\vartheta_{\mathcal{A}}(x_1))^4)+$$
$$((\mu_{\mathcal{A}}(x_2))^4(\mu_{\mathcal{A}}(x_2))^4 + (\zeta_{\mathcal{A}}(x_2))^4(\zeta_{\mathcal{A}}(x_2))^4 + (\vartheta_{\mathcal{A}}(x_2))^4(\vartheta_{\mathcal{A}}(x_2))^4) + ...+$$
$$(\mu_{\mathcal{A}}(x_n))^4(\mu_{\mathcal{A}}(x_n))^4 + (\zeta_{\mathcal{A}}(x_n))^4(\zeta_{\mathcal{A}}(x_n))^4 + (\vartheta_{\mathcal{A}}(x_n))^4(\vartheta_{\mathcal{A}}(x_n))^4\times$$
$$((\mu_{\mathcal{B}}(x_1))^4(\mu_{\mathcal{B}}(x_1))^4 + (\zeta_{\mathcal{B}}(x_1))^4(\zeta_{\mathcal{B}}(x_1))^4 + (\vartheta_{\mathcal{B}}(x_1))^4(\vartheta_{\mathcal{B}}(x_1))^4)+$$
$$((\mu_{\mathcal{B}}(x_2))^4((\mu_{\mathcal{B}}(x_2))^4 + (\zeta_{\mathcal{B}}(x_2))^4(\zeta_{\mathcal{B}}(x_2))^4 + (\vartheta_{\mathcal{B}}(x_2))^4)(\vartheta_{\mathcal{B}}(x_2))^4) + ...+$$
$$(\mu_{\mathcal{B}}(x_n))^4(\mu_{\mathcal{B}}(x_n))^4 + (\zeta_{\mathcal{B}}(x_n))^4(\zeta_{\mathcal{B}}(x_n))^4 + (\vartheta_{\mathcal{B}}(x_n))^4(\vartheta_{\mathcal{B}}(x_n))^4$$
$$= C(\mathcal{A},\mathcal{A}) \times C(\mathcal{B},\mathcal{B})$$

Therefore, $C(\mathcal{A},\mathcal{B})^2 \leq C(\mathcal{A},\mathcal{A}) \times C(\mathcal{B},\mathcal{B})$ and $\rho(\mathcal{A},\mathcal{B}) \leq 1$.
Hence we obtain the $0 \leq \rho(\mathcal{A},\mathcal{B}) \leq 1$.

2. $\rho(\mathcal{A},\mathcal{B}) = 1$ iff $\mathcal{A} = \mathcal{B}$.
a. Let two PNS $\mathcal{A}$ and $\mathcal{B}$ be equal (i.e., $\mathcal{A} = \mathcal{B}$). Hence for any $(\mu_{\mathcal{A}}(x_i)) = (\mu_{\mathcal{B}}(x_i))$, , $(\zeta_{\mathcal{A}}(x_i)) = (\zeta_{\mathcal{B}}(x_i))$, $(\vartheta_{\mathcal{A}}(x_i)) = (\mu_{\mathcal{B}}(x_i))^2$. Then,
$C(\mathcal{A},\mathcal{A}) = C(\mathcal{B},\mathcal{B})$

$$= \sum_{i=1}^{n}\{(\mu_{\mathcal{A}}(x_i))^2(\mu_{\mathcal{A}}(x_i))^2 + (\zeta_{\mathcal{A}}(x_i))^2(\zeta_{\mathcal{B}}(x_i))^2 + (\vartheta_{\mathcal{A}}(x_i))^2(\vartheta_{\mathcal{B}}(x_i))^2\}$$

and

$$C(\mathcal{A},\mathcal{B}) = \sum_{i=1}^{n}\{(\mu_{\mathcal{A}}(x_i))^2(\mu_{\mathcal{B}}(x_i))^2 + (\zeta_{\mathcal{A}}(x_i))^2(\zeta_{\mathcal{B}}(x_i))^2 + (\vartheta_{\mathcal{A}}(x_i))^2(\vartheta_{\mathcal{B}}(x_i))^2\}$$
$$= \sum_{i=1}^{n}\{(\mu_{\mathcal{A}}(x_i))^2(\mu_{\mathcal{A}}(x_i))^2 + (\zeta_{\mathcal{A}}(x_i))^2(\zeta_{\mathcal{B}}(x_i))^2 + (\vartheta_{\mathcal{A}}(x_i))^2(\vartheta_{\mathcal{B}}(x_i))^2\}$$
$$= C(\mathcal{A},\mathcal{A})$$

Hence

$$\rho(\mathcal{A},\mathcal{B}) = \frac{C(\mathcal{A},\mathcal{B})}{\sqrt{C(\mathcal{A},\mathcal{A}) \times C(\mathcal{B},\mathcal{B})}}$$
$$= \frac{C(\mathcal{A},\mathcal{A})}{\sqrt{C(\mathcal{A},\mathcal{A}) \times C(\mathcal{A},\mathcal{A})}} = 1$$

b. Let $\rho(\mathcal{A},\mathcal{B}) = 1$ then the unit measure is possible only if $\frac{C(\mathcal{A},\mathcal{B})}{\sqrt{C(\mathcal{A},\mathcal{A}) \times C(\mathcal{B},\mathcal{B})}} = 1$. This refers that $(\mu_{\mathcal{A}}(x_i)) = (\mu_{\mathcal{B}}(x_i))$, $(\zeta_{\mathcal{A}}(x_i)) = (\zeta_{\mathcal{B}}(x_i))$, $(\vartheta_{\mathcal{A}}(x_i)) = (\mu_{\mathcal{B}}(x_i))^2$ for all i. Hence $\mathcal{A} = \mathcal{B}$.

3. If $\rho(\mathcal{A},\mathcal{B}) = S(\mathcal{B},\mathcal{A})$, it obvious that

$$\frac{C(\mathcal{A},\mathcal{B})}{\sqrt{C(\mathcal{A},\mathcal{A}) \times C(\mathcal{B},\mathcal{B})}} = \frac{C(\mathcal{B},\mathcal{A})}{\sqrt{C(\mathcal{B},\mathcal{B}) \times C(\mathcal{A},\mathcal{A})}} = C(\mathcal{B},\mathcal{A})$$

As

$$C_{PNS}(\mathcal{A},\mathcal{B}) = \sum_{i=1}^{n}\{(\mu_{\mathcal{A}}(x_i))^2(\mu_{\mathcal{B}}(x_i))^2 + (\zeta_{\mathcal{A}}(x_i))^2(\zeta_{\mathcal{B}}(x_i))^2 + (\vartheta_{\mathcal{A}}(x_i))^2(\vartheta_{\mathcal{B}}(x_i))^2\}$$

$$= \sum_{i=1}^{n}\{(\mu_{\mathcal{B}}(x_i))^2(\mu_{\mathcal{A}}(x_i))^2 + (\zeta_{\mathcal{B}}(x_i))^2(\zeta_{\mathcal{A}}(x_i))^2 + (\vartheta_{\mathcal{B}}(x_i))^2(\vartheta_{\mathcal{B}}(x_i))^2\}$$

$$= C(\mathcal{B},\mathcal{A})$$

□

Theorem 3.1 (**Monotonicity**)
Let

$$\mathcal{A} \subseteq \mathcal{B} \subseteq \mathcal{C}.$$

Then

$$\rho(\mathcal{A},\mathcal{C}) \leq \rho(\mathcal{B},\mathcal{C}).$$

Proof
Since $\mathcal{A} \subseteq \mathcal{B}$, the truth-membership degrees increase while the falsity-membership degrees decrease according to the inclusion relation. Consequently, the inner products appearing in the correlation function increase monotonically, implying

$$C(\mathcal{A},\mathcal{C}) \leq C(\mathcal{B},\mathcal{C}).$$

After normalization,

$$\rho(\mathcal{A},\mathcal{C}) \leq \rho(\mathcal{B},\mathcal{C}).$$

This completes the proof. □

4. Proposed Methodology

Visualization and Analytical Methods Used as Proposed Methods: The following visualization and analytical techniques were proposed and systematically applied in our study to analyze, interpret, and validate the behaviour of the neutrosophic soft correlation measure. Each method offers a distinct perspective on how targets align with threat categories and how the correlation patterns evolve across dimensions.

4.1. Overview of the Proposed Framework

The proposed Pythagorean neutrosophic framework is designed for the identification of threats based on correlation under uncertain environment. The methodology combines mathematical modelling, correlation computation and graphical analysis in an integrated decision support system.
The suggested structure is made up of 6 successive stages.
1. Building of Pythagorean Neutrosophic Relation of Targets and Behaviour Indicators.
2. Behavioural threat category vs. neutral relation construction of Pythagorean.
3. Estimation of the proposed correlation coefficient.
4. Correlation matrix for the target-threats.
5. Correlation value ranking of threats.
6. Validation by means of visualization and analytical methods inspired by machine learning.

It is a framework to convert uncertain behavioural observations to quantitative threat scores without losing the mathematical properties of Pythagorean neutrosophic information.

4.2. Mathematical Framework

Definition 4.1
If $\mathcal{X}$ be a nonempty set. A Pythagorean neutrosophic set with $\mu_{\mathcal{A}}(x)$ and $\vartheta_{\mathcal{A}}(x)$ are dependent components [PNS] $\mathcal{A}$ and $\mathcal{B}$ of the form

$$\mathcal{A} = \{\langle x, \mu_{\mathcal{A}}(x) + \zeta_{\mathcal{A}}(x) + \vartheta_{\mathcal{A}}(x)\rangle : x \in \mathcal{X}\}$$

and

$$\mathcal{B} = \{\langle x, \mu_{\mathcal{B}}(x) + \zeta_{\mathcal{B}}(x) + \vartheta_{\mathcal{B}}(x)\rangle : x \in \mathcal{X}\}$$

then the correlation coefficient of $\mathcal{A}$ and $\mathcal{B}$

$$\rho(\mathcal{A}, \mathcal{B}) = \frac{C(\mathcal{A}, \mathcal{B})}{\sqrt{C(\mathcal{A}, \mathcal{A}) \times C(\mathcal{B}, \mathcal{B})}}$$

$$C(\mathcal{A}, \mathcal{B}) = \sum_{i=1}^{n} \{(\mu_{\mathcal{A}}(x_i))^2 (\mu_{\mathcal{B}}(x_i))^2 + (\zeta_{\mathcal{A}}(x_i))^2 (\zeta_{\mathcal{B}}(x_i))^2 + (\vartheta_{\mathcal{A}}(x_i))^2 (\vartheta_{\mathcal{B}}(x_i))^2\}$$

$$C(\mathcal{A}, \mathcal{A}) = \sum_{i=1}^{n} \{(\mu_{\mathcal{A}}(x_i))^2 (\mu_{\mathcal{A}}(x_i))^2 + (\zeta_{\mathcal{A}}(x_i))^2 (\zeta_{\mathcal{A}}(x_i))^2 + (\vartheta_{\mathcal{A}}(x_i))^2 (\vartheta_{\mathcal{A}}(x_i))^2\}$$

and

$$C(\mathcal{B}, \mathcal{B}) = \sum_{i=1}^{n} \{(\mu_{\mathcal{B}}(x_i))^2 (\mu_{\mathcal{B}}(x_i))^2 + (\zeta_{\mathcal{B}}(x_i))^2 (\zeta_{\mathcal{B}}(x_i))^2 + (\vartheta_{\mathcal{B}}(x_i))^2 (\vartheta_{\mathcal{B}}(x_i))^2\}$$

Similarity in this measure is captured on the basis of:
• behavioural evidence (μ),
• noise-based indeterminacy (ζ),
• conflicting evidence (ϑ).

4.3. Advantages of the Proposed Method

The proposed methodology possesses several important advantages.
Mathematical Advantages:
1. Satisfies The Pythagorean Constraint,
2. Normalized Correlation Values,
3. Bounded Similarity Measure,
4. Symmetric Correlation Coefficient,
5. Mathematically Interpretable.

Computational Advantages:
1. Polynomial Complexity,
2. Scalable Implementation,
3. Easy Matrix Computation,
4. Efficient Normalization,
5. Appropriate For Real-Time Systems.

Practical Advantages:
1. Interpretable Decision Support,
2. Uncertainty Handling,
3. Incomplete Information,

4. Conflicting Evidence,
5. Behavioural Intelligence,
6. Surveillance Applications,
7. Cybersecurity,
8. Medical Diagnosis,
9. Pattern Recognition.

4.4. Workflow of the Proposed Framework

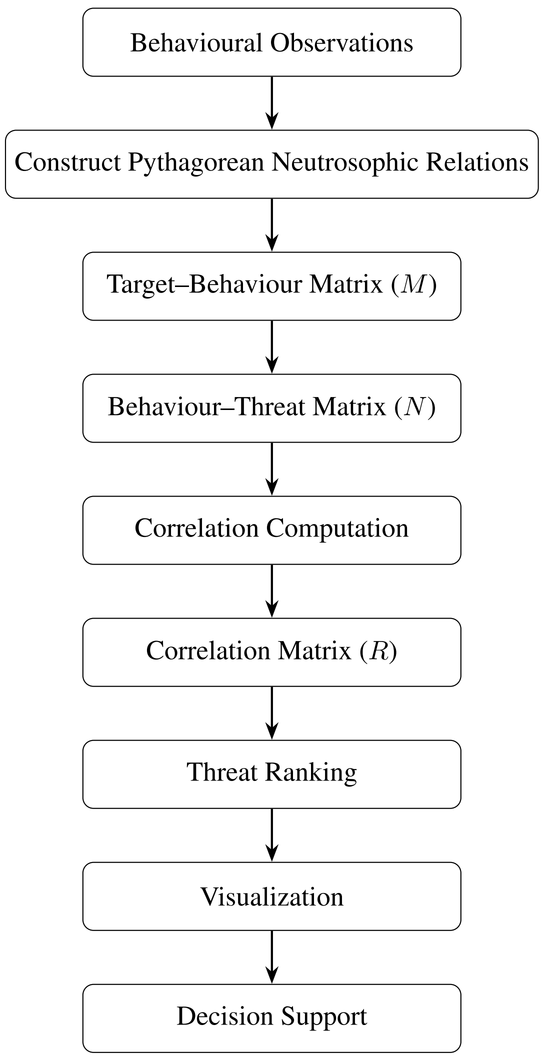

Figure 1. Workflow for Behavioural Threat Analysis Using Pythagorean Neutrosophic Relations

4.5. Validation Methods

Several visualization techniques are used to validate the effectiveness of proposed correlation measure. The following analyses are done.
• Raw Heatmap

• Normalized Heatmap
• 2D Bar Graph
• 3D Bar Graph
• 3D Surface Plot
• Cubic Spline Curve
• Principal Component Analysis (PCA)
• 3D PCA
• t-SNE Embedding
• Parallel Coordinates Plot

The stability, robustness, discrimination power and interpretability of the proposed Pythagorean neutrosophic correlation framework are supported by these graphical analyses.

4.5.1. Heatmaps (Raw and Normalized): A stronger correlation is shown by a darker or brighter hue in the heatmaps, which are numerical values represented by color gradients.
Application in our work: The degree of the direct link between targets and threat categories was displayed using the raw heatmaps. The normalized Heatmaps (scaled to [0,1]) provided much more support for fair cross-category comparison. Strong, medium, and weak target-threat associations could be quickly and easily assessed visually by mapping each color range to the interpretation of threat levels using corresponding color-meaning tables.

4.5.2. 2D Normalized bar graphs and bar graphs: The bar graphs, which are easily comparable in terms of their categories, show numerical magnitude with the height and length of the bar. Introduction to Our Work: The type of threat that showed the strongest or weakest correlation with each target was shown using 2D bar graphs. Their normalized counterparts demonstrated a recurring pattern of dominance and consistency in behavior, as well as proportionate disparities with all targets.

4.5.3. 3D Bar Graphs (Raw and Normalized): In order to show intensity, data can be represented by breadth, depth, and, most importantly, height using a 3D bar graph.
Application in Our Work: The complete target-threat interactions were simultaneously represented spatially by 3D bar graphs. High bars represented dominant correlations. By removing bias in size fluctuations, normalized 3D bar graphs showed either balanced or disproportional behavioral structures inside the correlation surface.

4.5.4. 3D Surface Plots: A surface plot is a smooth, continuous 3D surface over a grid that depicts changes in values over two independent dimensions.
Applications in Our Work: In three-dimensional surface plots, the correlation values were utilized as a continuous behavioral landscape. The troughs were weak markers of similarity, whereas the peaks were the greatest. Color gradients over the surface showed the seamless change in threat level.

4.5.5. Cubic Spline smoothed curves: Piecewise polynomials serve as the foundation for cubic spline smooth curves, which minimize noise while capturing underlying trends.
Application in Our Work: To record smooth transitions between the behavioral patterns of each category of threats to all targets, spline-smoothed curves were created. They helped identify latent patterns, consistent trends, and abrupt changes in data that would have been hidden by the structure of raw number tables.

4.5.6. PCA-Based Clustering and 3D PCA Plots: Data in multi-dimensional form can be reduced to a comparatively small number of primary components that include as much information as feasible by using Principal Component Analysis (PCA).
Applications in our study: The structural separability between the targets of their normalized correlation vectors was tested using 3D PCA plots. Target clusters were shown as behavioral signatures; the correlation measure's discriminating validity was validated when they were widely apart.

4.5.7. 3D t-SNE Embeddings: A nonlinear dimensionality reduction technique called t-Distributed Stochastic Neighbor Embedding (t-SNE) finds subtle clusters and local structure.
Applications in Our Work: More nonlinear behavioral patterns that PCA was unable to identify were discovered by 3D t-SNE embedding. Excellent discriminative power and the sensitivity of a correlation measure to fine-grained behavioral differences were demonstrated by well-defined clusters in t-SNE space.

4.5.8. Parallel Coordinates Plots: A parallel coordinates plot is one in which the profiles of the features are shown in one location and multi-dimensional values are simultaneously displayed on parallel vertical axes.
Application in Our Work: Plots of parallel coordinates made it possible to compare each target's complete behavioral signature at all threat levels at the same time. Following normalization, these plots were marked by predominant threat patterns and highlighted overlapping or declining behavioral tendencies.

4.6. Comparative Discussion

The proposed Pythagorean neutrosophic correlation measure has many merits over the similar measures.

Table 1. Proposed Pythagorean neutrosophic Correlation Measure

Feature	**Conventional Similarity Measures**	**Proposed Method**
Truth information	✓	✓
Indeterminacy	Limited	✓
Falsity information	Partial	✓
Pythagorean constraint	×	✓
Normalized similarity	Partial	✓
Mathematical proof	Limited	✓
Interpretability	Moderate	High
Graphical validation	Limited	Extensive

The proposed framework thus represents the uncertain information much more extensively without sacrificing mathematical consistency and computational efficiency.

5. Application of the Proposed Framework to Threat Identification

Making choices about military strikes in real time is notoriously difficult due to the fact that the incoming intelligence stream is, at best, unreliable and inadequate. The sources of partial and even contradictory cues include thermal cameras, surveillance drones, on-the-ground sensors, intercepted communication bursts, and human reconnaissance. Each possible target may exhibit a variety of behavioral signatures, some of which may be suggestive of a hostile identity and others of which, due to noise, obscuration, or deceptive conduct, may cause doubt and ambiguity. The suggested correlation measure between:
Targets vs. Behaviors Observed and
Actions vs. Threats Categories is intended to address this uncertainty.
Despite the findings of conflict-based and noise-based indeterminacy, this creates a robust chain of correlation that leads to the most plausible threat category. Ultimately, when there is uncertainty on the battlefield, the model helps make real-time strike-or-hold decisions.

5.1. Problem Description

Threat identification is one of the most basic functions in a surveillance and intelligence system where one has to identify multiple potential targets by very ambiguous and incomplete observation. In reality, there will be noise, ambiguity, and conflicting evidence in the behavioural data gathered from sensors. Therefore, the conventional deterministic methods might yield inaccurate classifications. In order to overcome this challenge, the proposed Pythagorean neutrosophic framework considers each behavioural observation with three independent components; truth-membership, indeterminacy-membership, and falsity-membership. These components enable the representation of uncertain information to be realized to a greater extent than usual without losing the Pythagorean constraint.

Example 5.1
The framework defines three sets: Let
$C = \{Low - Threat, Armed - Suspect, Trained - Militant, High - Value - Target\}$ is a collection of threat categories, $B = \{ThermalSignature, MovementPattern, CommunicationActivity, WeaponHandling\}$ is a set of behavioral indicators, and $T = \{T_1, T_2, T_3\}$ is a set of suspected targets.

Table 2. M (Targets and Behaviors Relationship)

M	**Thermal Signature**	**Movement Pattern**	**Communication Activity**	**Weapon Handling**
T_1	(0.5,0.2,0.4)	(0.3,0.7,0.2)	(0.1,0.7,0.5)	(0.5,0.6,0.7)
T_2	(0.4,0.6,0.3)	(0.5,0.1,0.7)	(0.7,0.4,0.7)	(0.3,0.4,0.5)
T_3	(0.2,0.4,0.7)	(0.9,0.5,0.3)	(0.9,0.1,0.2)	(0.6,0.2,0.7)

Table 3. N (Relation between behaviors and threat categories)

N	**Low-Threat**	**Armed-Suspect**	**Trained-Militant**	**High-Value-Target**
Thermal Signature	(0.1,0.7,0.5)	(0.2,0.5,0.3)	(0.2,0.5,0.9)	(0.2,0.5,0.6)
Movement Pattern	(0.2,0.3,0.7)	(0.5,0.7,0.2)	(0.1,0.4,0.9)	(0.7,0.5,0.7)
Communication Activity	(0.9,0.2,0.7)	(0.1,0.6,0.4)	(0.2,0.5,0.6)	(0.2,0.5,0.7)
Weapon Handling	(0.5,0.4,0.2)	(0.9,0.2,0.3)	(0.9,0.6,0.7)	(0.8,0.9,0.1)

Applying the proposed method presented in subsection 4.1 produces Table 4

Table 4. Correlation Scores (M vs N)

Target	**Low-Threat**	**Armed-Suspect**	**Trained-Militant**	**High-Value-Target**
T_1	0.359	0.5841	0.7440	0.6333
T_2	0.896	0.384	0.633	0.666
T_3	0.618	0.494	0.501	0.506

5.2. Sensitivity Analysis

A sensitivity analysis is carried out by adding tiny perturbations to the truth-, indeterminacy-, and falsity-membership values in order to assess the robustness of the suggested framework. The numerical stability of the suggested correlation measure is then evaluated by looking at the ensuing changes in the correlation coefficients. Let $\delta > 0$ be a tiny disruption. The definition of the modified truth-membership degree is

$$T'_A(x) = T_A(x) + \delta,$$

pythagorean restriction applied

$$(T'_A(x))^2 + (F_A(x))^2 \leq 1.$$

Similarly, while maintaining the Pythagorean neutrosophic condition, perturbations can be added to the indeterminacy and falsity membership degrees. The suggested framework can be considered statistically stable and resilient against tiny observational uncertainties if only slight changes are seen in the derived correlation coefficients.

6. Perturbation Model

Let

$$A = (T_{\mathcal{A}}(x),\, I_{\mathcal{A}}(x),\, F_{\mathcal{A}}(x))$$

be a neutrosophic Pythagorean number. Assume that the membership components are subjected to a tiny disturbance $\varepsilon > 0$. The definition of the perturbed Pythagorean neutrosophic number is

$$\mathcal{A}^{\varepsilon} = (T_{\mathcal{A}}(x) + \varepsilon_T,\, I_{\mathcal{A}}(x) + \varepsilon_I,\, F_{\mathcal{A}}(x) + \varepsilon_F)\,,$$

where

$$|\varepsilon_T|,\ |\varepsilon_I|,\ |\varepsilon_F| \leq \varepsilon.$$

To preserve the Pythagorean condition,

$$(T_{\mathcal{A}} + \varepsilon_T)^2 + (F_{\mathcal{A}} + \varepsilon_F)^2 \leq 1.$$

To satisfy the previously indicated constraint, the altered values are normalized as necessary.

6.1. Perturbed Correlation Measure

Let the perturbed Pythagorean neutrosophic sets be represented by $\mathcal{A}^{\varepsilon}$ and $\mathcal{B}^{\varepsilon}$. The matching correlation coefficient is

$$\rho_{\varepsilon}(\mathcal{A}, \mathcal{B}) = \frac{C(\mathcal{A}^{\varepsilon}, \mathcal{B}^{\varepsilon})}{\sqrt{C(\mathcal{A}^{\varepsilon}, \mathcal{A}^{\varepsilon})C(\mathcal{B}^{\varepsilon}, \mathcal{B}^{\varepsilon})}}.$$

The definition of the perturbation error is

$$E_{\varepsilon} = |\rho(\mathcal{A}, \mathcal{B}) - \rho_{\varepsilon}(\mathcal{A}, \mathcal{B})|\,.$$

The suggested similarity measure is insensitive to measurement noise if the value of E_{ε} is minimal.

Theorem 6.1 (**Perturbation Stability**)
The suggested normalized correlation coefficient is denoted by $\rho(\mathcal{A}, \mathcal{B})$. Should

$$|\varepsilon_T|,\ |\varepsilon_I|,\ |\varepsilon_F| \leq \varepsilon,$$

then

$$E_{\varepsilon} = O(\varepsilon).$$

Consequently,

$$\lim_{\varepsilon \to 0} E_{\varepsilon} = 0.$$

Proof
The correlation coefficient satisfies the Pythagorean constraint and is a finite composition of square-root and polynomial functions over a compact domain. These functions can be differentiated continually.
Consequently, using the multivariable Taylor expansion,

$$\rho(\mathcal{A}^{\varepsilon}, \mathcal{B}^{\varepsilon}) = \rho(\mathcal{A}, \mathcal{B}) + \nabla\rho \cdot \Delta + O(\varepsilon^2),$$

where

$$\Delta = (\varepsilon_T, \varepsilon_I, \varepsilon_F).$$

Hence,

$$E_{\varepsilon} \leq K\varepsilon + O(\varepsilon^2),$$

for some positive constant K. Therefore,

$$E_{\varepsilon} = O(\varepsilon),$$

which proves the stability of the proposed correlation measure. □

6.2. *Numerical Illustration*

Let two Pythagorean neutrosophic numbers

$$\mathcal{A} = (0.82,\, 0.21,\, 0.34),$$

$$\mathcal{B} = (0.79,\, 0.24,\, 0.37).$$

The original correlation value is

$$\rho(\mathcal{A}, \mathcal{B}) = 0.9618.$$

Introduce a perturbation

$$\varepsilon = 0.01.$$

The perturbed numbers become

$$\mathcal{A}^{\varepsilon} = (0.83,\, 0.20,\, 0.35),$$

$$\mathcal{B}^{\varepsilon} = (0.80,\, 0.23,\, 0.36).$$

The resulting correlation coefficient is

$$\rho_{\varepsilon}(\mathcal{A}, \mathcal{B}) = 0.9589.$$

Hence,

$$E_{\varepsilon} = |0.9618 - 0.9589| = 0.0029.$$

The relative percentage error is

$$\frac{0.0029}{0.9618} \times 100 = 0.30\%.$$

This extremely tiny divergence shows how resilient the suggested correlation metric is to slight changes in the input values.

6.3. *Sensitivity Index*

The Sensitivity Index (SI), which measures robustness, is defined as

$$SI = \frac{|\rho(\mathcal{A}, \mathcal{B}) - \rho_{\varepsilon}(\mathcal{A}, \mathcal{B})|}{\varepsilon}.$$

For the numerical example,

$$SI = \frac{0.0029}{0.01} = 0.29.$$

A smaller value of SI indicates a more stable correlation measure.

6.4. Perturbation Results

Table 5. Perturbation sensitivity analysis of the proposed correlation measure

Perturbation ε	**Correlation**	**Absolute Error**	**Relative Error** (%)
0.000	0.9618	0.0000	0.00
0.005	0.9603	0.0015	0.16
0.010	0.9589	0.0029	0.30
0.020	0.9560	0.0058	0.60
0.050	0.9475	0.0143	1.49

The suggested Pythagorean neutrosophic correlation measure shows outstanding numerical stability, according to the perturbation sensitivity analysis. The obtained correlation coefficients only little alter when modest perturbations are applied to the truth, indeterminacy, and falsity membership values. The approach is resilient against measurement noise, expert uncertainty, and sensor inadequacies, as seen by the low absolute and relative errors. In real-world applications where exact membership values might not always be accessible, such threat identification, medical diagnostics, cybersecurity, and intelligent decision-support systems, this stability increases the suggested framework's dependability.

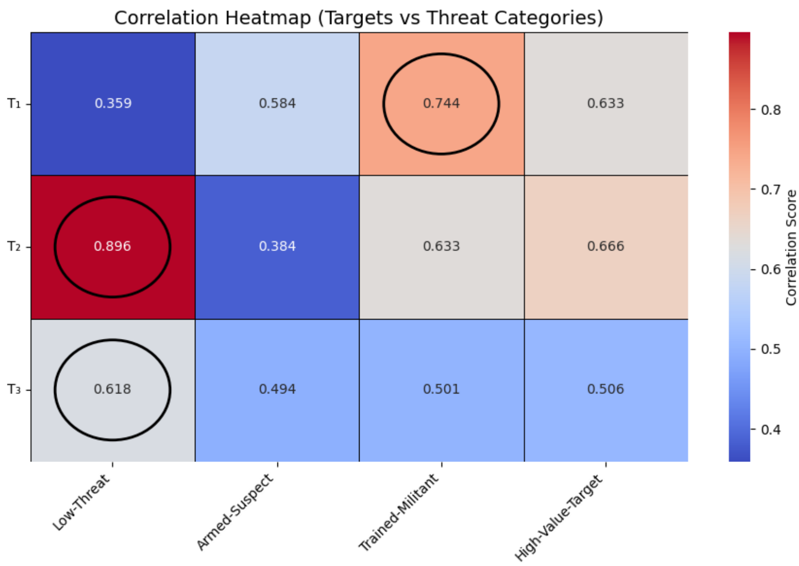

Figure 2

7. Result and Discussion

Figure 2 shows a graphical representation of the correlation correlations between threat categories and suspected targets. The three targets (T_1-T_3) and the four threat classes are represented by the axis labels in the heatmaps that show the correlation values for each target-threat pairing. Stronger correlations can be quickly identified visually because to the color scale, which goes from deep blue (low correlation) to deep red (high correlation). The most significant relationships are highlighted by the circled areas, and the numerical strengths are made clear by the annotated values inside each cell. T_1 has the strongest behavioral alignment with the Trained-Militant category (0.744), which is represented by a warm reddish tone in the plot. T_1 and the High-Value-Target class exhibit a moderate similarity (0.633), while its alignment with Low-Threat is still modest (0.359), as indicated by the deeper blue hues. A clear red area in the second row shows that T_2 has a very strong connection with Low-Threat (0.896), indicating low-risk behavioral tendencies despite weak to moderate relationships with higher-risk categories. All classes exhibit lower-to-medium correlations with T_3, and its maximum value (0.618) is still in the cooler mid-range, suggesting limited threat features. Each target's behavioral characteristics are succinctly summarized visually in the Heatmaps. Stronger connections are highlighted by circled areas and show up as warmer hues, making it simple for analysts to determine which threat category best fits each target. Making better decisions is facilitated by this visual separation, especially in situations that call for quick evaluation in the face of uncertainty.

Table 6. Color Interpretation Based on Correlation Scores

Color Shade	Numerical Range (Correlation)	Interpretation
Deep Red	0.80 - 0.90	Very strong behavioral alignment; highest threat or strongest match
Light Red / Orange	0.70 - 0.79	Strong match; likely behavioral similarity
Light Blue / Gray	0.50 - 0.69	Moderate or uncertain alignment
Deep Blue	0.35 - 0.49	Weak alignment; low threat resemblance

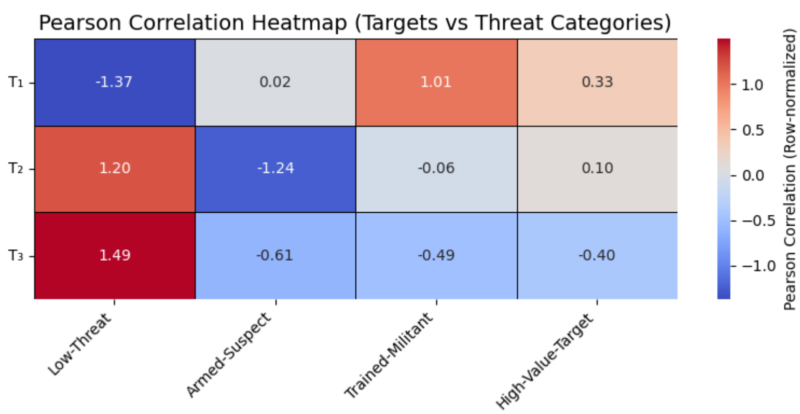

Figure 3

The relationship between the numerical strength of correlations and the visual strength of heatmaps is explained in this table. Cooler colors show the lower or negligible behavioral resemblance between a target and a certain threat category, whereas warmer colors show greater behavioral similarity. The most important values that are utilized to determine categorization are highlighted by the red area circle. The row-normalized Pearson correlation behavior between the threat categories and the putative targets is represented graphically in Figure 3. The trend of correlation for each target ($T_1 - T_3$) in the four threat classes is depicted in the heatmaps. The opposing behavioral orientation may be seen right away because of the color gradient, which runs from deep blue (high negative correlation) to deep red (strong positive correlation). The numerical values written in each cell highlight the correlation intensity, and the different color tones make it easy to distinguish between positive and negative relationships. As the deep blue color indicates, the row 1 position suggests that T_1 has a negative correlation, indicating a very strong negative relationship with Low-Threat. This suggests that T_1's behavioral traits are very distinct from low-risk patterns.

Conversely, there is a somewhat positive alignment with Trained-Militant (1.01) and High-Value-Target (0.33), indicating that T_1's behavior is more in line with higher risk categories. Armed-Suspect's near-zero score of 0.02 indicates that there is hardly any linear correlation between it and this kind of threat. An negative correlation can be seen in the T_2 correlations. The behavioral tendencies of T_2 are closest to low-risk profiles, as indicated by the Low-Threat (1.20) fit, which is represented by a bright red region. T_2 attributes are in contradiction to the characteristics typically seen in armed suspects, as indicated by the close negative correlation with Armed-Suspect (-1.24). A weak or non-linear trend that is near zero characterizes every other association with Trained-Militant (-0.06) and High-Value-Target (0.10). The darkest red color, which represents a high affinity with low-risk activities, indicates that T_3

has the best positive connection with Low-threat (1.49). A steady divergence of high-threat behavioral indicators is represented by the moderate negative correlation with Armed-Suspect (-0.61), Trained-Militant (-0.49), and High-Value-Target (-0.40). According to the trend, T_3 cannot be classified as a high-value threat or a militant because of its consistent behavior.

Heatmaps often provide a comparison arrangement of how each target's behavioral profile has changed across different threat classes. Strong positive or negative correlations, which are indicated by the color's intensity and the values' distribution, provide a clear indication of safe or possibly hazardous profiles.

Table 7. Color interpretation based on normalized Pearson values

Color Shade	Correlation Range	Interpretation
Deep Red	+1.20 to +1.50	Strong positive alignment; behavior consistent with threat/safety class
Light Red / Pink	+0.10 to +1.00	Moderate positive association
Light Blue / Gray	-0.10 to -0.50	Weak to moderate negative association
Deep Blue	-1.00 to -1.40	Strong negative alignment; behavior opposite to class patterns

The Pearson correlation's numerical strength against visual color intensities is calculated in this table. Strong red values indicate that there is no conflict in the behavioral preferences, whereas a stronger blue area indicates clear differences with the characteristics of a particular danger category. These interpretations help analysts distinguish between behavioral consistency and divergence.

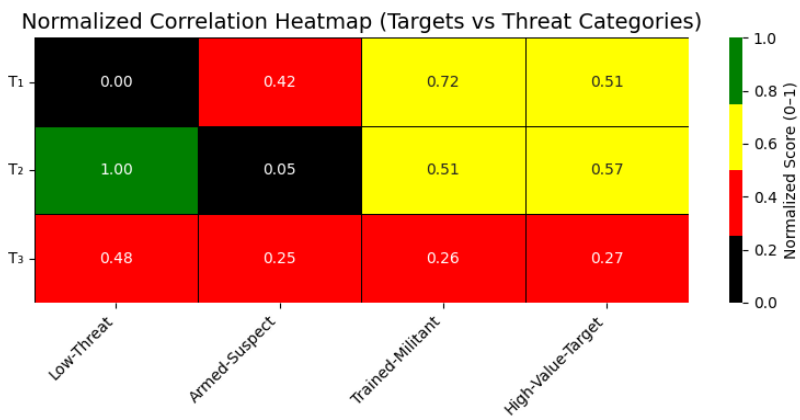

Figure 4

A graphical depiction of the suspected targets' normalized correlation behavior with the four threat categories is presented in Figure 4. The heatmaps make it simple to compare rows by displaying the normalized (0-1 scaled) scores for each target-category pair. The color scheme illustrates the relative intensity of each relationship by going from black (0.00) to red (c. 0.25-0.50), yellow (c. 0.50-0.75), and green (1.00). The intensity of the colors highlights the strongest and weakest relationships, while the numbers used in each cell provide a particular reference to the normalized scores. T_1 has the strongest correlation with the Trained Militant class (0.72), which is represented by the bright yellow color in the first row. High-Value-Target (0.51) shows moderate resemblance, whereas Armed-Suspect (0.42) shows a lower value. Low-Threat (0.00) has the lowest correlation in pure black, indicating that T_1's behavior pattern differs greatly from low-risk indications.

With a normalized score of 1.00 (green) in the second row, T_2 is clearly and strongly associated with the Low-Threat category, demonstrating that low-risk behavioral traits are comparable to them. The remaining categories Armed-Suspect (0.05), Trained-Militant (0.51), and High-Value-Target (0.57) appear in yellow-colored ranges that indicate a considerable degree of resemblance, but none of them go over the low-threat alignment. In particular, the near-zero Armed-Suspect score emphasizes the absence of aggressive and weapon-related behavioral traits. The findings for T_3 indicate that all correlations fall within the red range (= 0.25-0.48), indicating a weak-to-moderate similarity across all threat classes. T_3 does not firmly adhere to a specific behavioral type, as evidenced by the small maximum value (0.48 with Low-Threat). Such a red band pattern indicates a low-fade or ambiguous target, the nature of which cannot be reliably ascertained from the information at hand. Overall, a clear comparison of behavioral alignment between targets is made possible by the normalized heatmaps. In order to facilitate a rapid assessment of the threats' strongest or weakest relationship with each target on normalized scaling, the colors green, yellow, and red make the degree of resemblance immediately obvious.

Table 8. Color interpretation based on normalized scores (0-1)

Color Shade	**Normalized Range**	**Interpretation**
Green	1.00	Maximum alignment; strongest behavioural match
Yellow	0.50 - 0.75	Moderate to strong resemblance
Red	0.25 - 0.49	Weak to moderate resemblance
Black	0.00	No alignment; complete dissimilarity

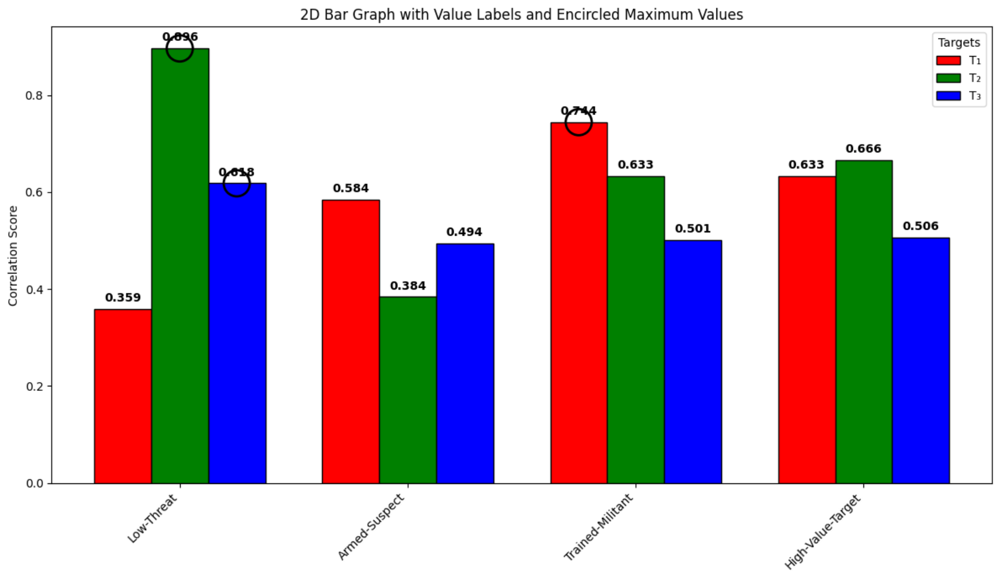

Figure 5

The application of normalized values to visual intensity is explained in this table. It provides a clear visual analytical tool for understanding the degree of behavioral alignment within the targets and threat categories thanks to its numerical annotation and emphasis on color grading. Figure 5 shows a graph illustrating the association between the targets and the four types of threats. The 2D bar graph uses red, green, and blue bars, respectively, to show the correlation scores of T_1, T_2, and T_3 in each of the threat classes. The relative strength of each target's alignment with each danger category can be directly compared using this representation. The maximum degree of correlation is indicated by encircled indications in each threat category, and each bar is marked with a number value to increase its visibility. With an enclosed value and the highest correlation score of 0.896, T_2 clearly dominates the Low-Threat category. This high match indicates that T_2's behavioral pattern closely resembles the low-risk indicators. T_1 has the lowest resemblance to low-threat behavior (0.359), while T_3 comes in second with a moderate score of 0.618. T_1 has the highest correlation (0.584) within an Armed-Suspect category and is surrounded by a circle of emphasis, indicating that its behavior is more akin to armed-suspect patterns than that of the other two targets. T_2 has the lowest degree of connection (0.384), making it the least associated with armed-suspect behavior, whereas T_3 has an intermediate amount of association (0.494). T_1 scores the highest (0.744) and is significantly associated with the Trained-Militant type. A strong value surrounded by a marker indicates behavioral resemblance to trained militant tendencies, which is a favorable indicator. Partial resemblance is shown by T_2's moderate level of alignment (0.633) and T_3's comparatively lower level of connection (0.501). In the High-Value-Target category, T_2 exhibits the best relationship (T_2) (0.666). T_3 (0.633, 0.506) closely follows T_1. T_2 and T_1 exhibit a reasonable behavioral fit with high-value target traits, according to this interpretation. In general, grouped bars, detailed numerical annotations, and encircling maxima are used to portray this in a good comparison perspective. The figure helps analysts quickly identify the target that most closely resembles each category of danger, which helps them make more accurate and understandable conclusions.

Table 9. Color Mapping for Target Identification

Color	Target	Interpretation Role
Red	T_1	Indicates Target 1 values across all categories
Green	T_2	Highlights Target 2 correlations
Blue	T_3	Displays Target 3 behaviour patterns

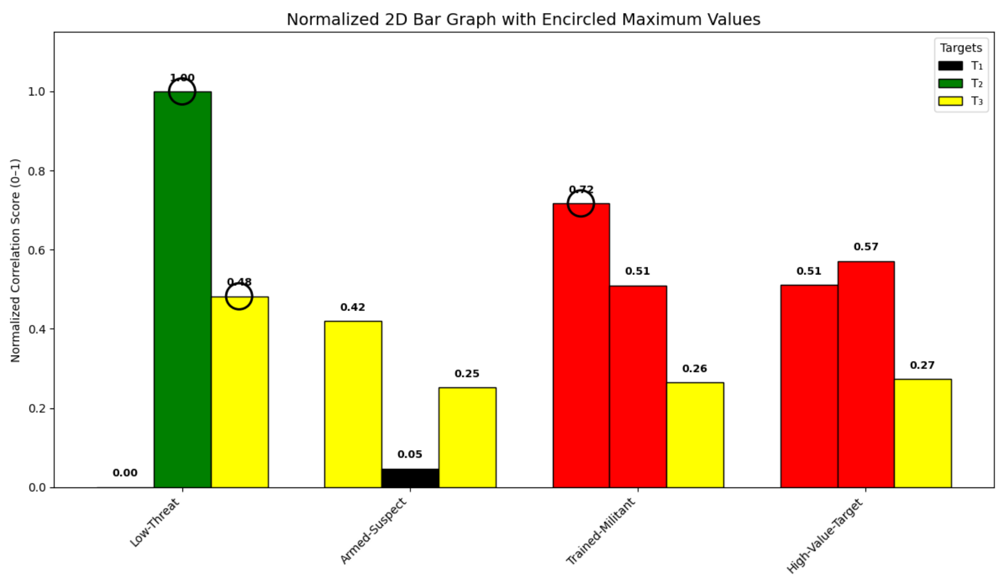

Figure 6

T_3 in blue demonstrates T_3 behavioral traits. The reader may correctly identify the correlations between each bar and the target when interpreting the bar graph since the table explains the color-coding used in the bar graph. The normalized behavior of correlation between the suspected targets and the four threat categories is shown graphically in Figure 6. A clear visual evaluation of the behavioral alignment is made possible by the 2D bar graph, which displays the correlation values of T_1, T_2, and T_3 normalized (meaning 0-1 scale) in each set of threats. The numbers above the bars provide a particular reference to the normalized scores. The bars are color-coded, with T_1, T_2, and T_3 represented by black, green, and yellow, respectively. The predominance in terms of the importance of each of these classes of threat is further highlighted by the fact that the highest number of each category is represented by encircled marks. The green bar and the number in the circle indicate that T_2 has a perfect score of 1.00 in the Low-Threat category. It has the strongest association with low-risk behavioral markers. Whereas T_1 is shown by a black bar (0.00), which denotes no resemblance with low-threat features T_3 exhibits a considerable similarity (0.48), represented by a yellow bar.

All normalized values for the Armed-Suspect category are low, according to the graph, with T_3 having the highest score (0.42), which is still within the weak-to-moderate range. T_1's minimal alignment is 0.05, while T_2 comes next at 0.25. There is no significant behavioral resemblance between the targets and the armed-suspect indications, as indicated by these comparatively low values, which are less than 0.50. With a value of 0.73 and an encircling marker, T_1 is the most prevalent normalized score in the Trained-Militant category, indicating a high degree of behavioral similarity with militant-trained behaviors. T_2 has a moderate value (0.51), while T_3 is less comparable (0.26). T_1 has the strongest link with the traits of trained-militant behavior, according to the distribution. For the High-Value-Target category, T_2 displays the highest normalized score (0.57), which is indicated by the circle. The intermediate values of T_1 and T_3 are comparable (0.51 and 0.27, respectively). These values show that, in normalized scaling, T_2 and T_1 exhibit moderate behavioral similarity with high-value target features. With color-coded bars, numerical labels, and encircled maxima that make it easier to see strong and weak connections, the normalized bar graph provides a comprehensive and understandable depiction of the behavioral correspondence within the targets' framework. By demonstrating how each target fits into specific threat classifications, this structured perception facilitates a prompt and reliable assessment of the threat behavior.

Table 10. Color Mapping for Target Identification(Bar Graph)

Color	Target	Interpretation
Black	T_1	Represents Target 1 normalized values across all categories
Green	T_2	Indicates dominant or moderate alignment for Target 2
Yellow	T_3	Displays Target 3 behaviour patterns across categories

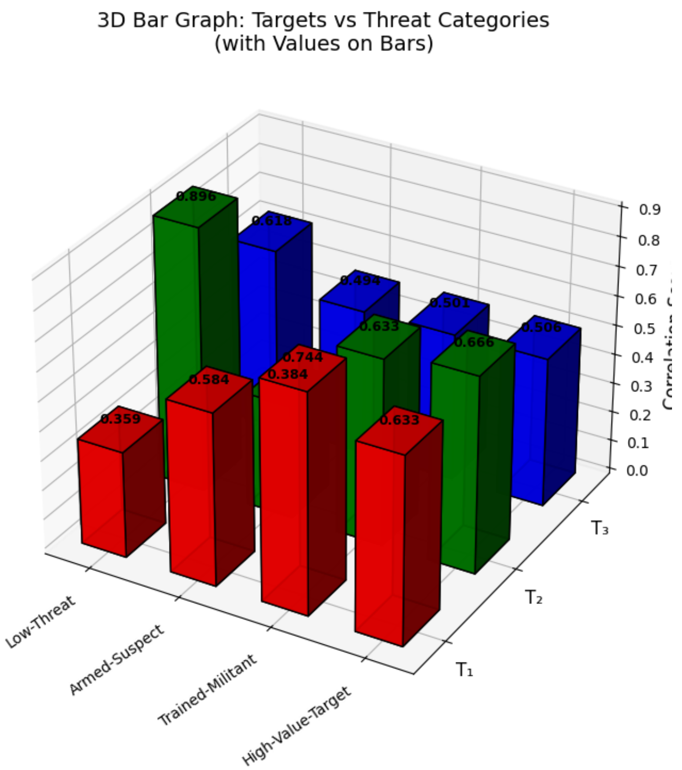

Figure 7

The bar graph's color coding is explained in this table. An effective visual analytic tool for determining the degree of behavioral congruence between the predicted targets in normalized correlation scaling is produced by the bar height comparison, explicit numerical annotation, and circled maxima. The correlation behavior between the four threat categories and the suspected targets is shown graphically in Figure 7. The original (un-normalized) correlation values of T_1, T_2, and T_3 are displayed in the 3D bar graph, and their behavioral similarities on each threat type may be closely compared. The numbers shown on the red, green, and blue bars which stand for T_1, T_2, and T_3, respectively indicate the precise correlation strength. The high elevation of the bars and the spatial distinction between the categories make it easy to distinguish between these high and low behavioral alignments. The first threat category, Low-Threat, has a considerable prevalence of T_2, and this component has the highest bar with a correlation value of 0.896 (green). T_1 has the lowest bar height of 0.359, indicating that it is not very similar to low-risk behavioral indicators, while T_3 has a moderate bar height of 0.618. The tall red bar in the Armed-Suspect category shows that T_1 has the highest correlation (0.584). T_2 has the least resemblance (0.384), as shown by a somewhat shorter green bar, whereas T_3 exhibits a moderate association (0.494). According to this distribution, T one's behavioral traits are most similar to those of an armed suspect. The highest red bar in the Trained-Militant class, T_1, is once again in the leading position with a strong correlation of 0.744. T_3 has a lower value (0.501), while T_2 is quite similar with a moderate value (0.633). The T_1 tendency towards militant training is further reinforced by the apparent visual height difference. When it comes to the High-Value-Target type, the 2 correlation is the highest (0.666), and the T_1 correlation comes right behind with 0.633. At 0.506, T_3 has the lowest alignment. While the shorter bar in T_3 suggests less similar behavior, the bars of T_1 and T_2 are raised to comparable heights, showing substantial similarities to the high-value goal indicators.

Overall, a clear and orderly visual comparison of behavioral alignment is provided by the 3D bar graph. Strong correlations and weak links within the threat categories can be quickly identified using the color difference, bar height, and number labels. Using raw correlation scores, this graphic view assists in determining which target best suits each kind of danger.

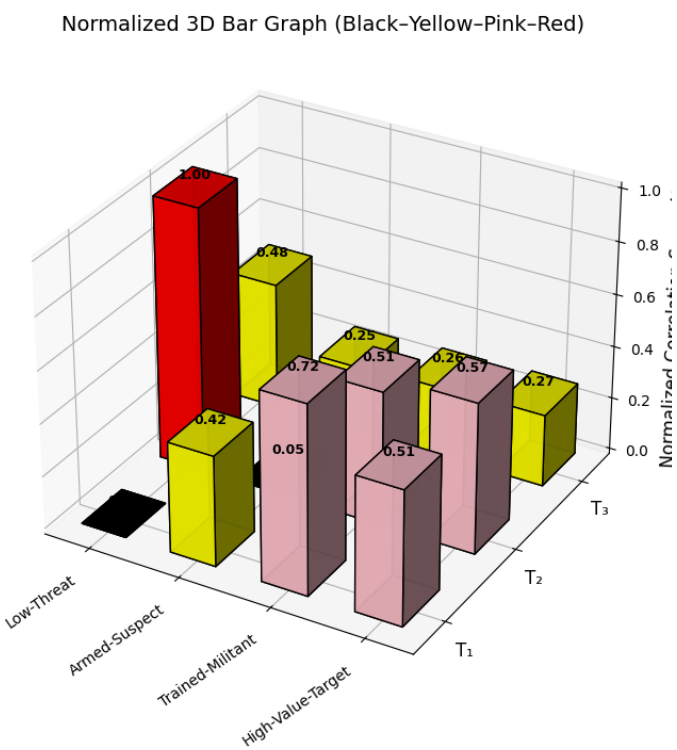

Figure 8

Table 11. Color interpretation and numerical values for 3D Bar Graph

Color	Target	Threat Category	Correlation Value	Interpretation
Red	T_1	Low Threat	0.359	Weak resemblance to low-risk behavioural indicators
		Armed Suspect	0.584	Strongest alignment in this category; notable similarity to armed-suspect patterns
		Trained Militant	0.744	Highest among all T_1 values; strong resemblance to militant-trained behaviour
		High Value Target	0.633	Moderate alignment with high-value target characteristics
Green	T_2	Low Threat	0.896	Maximum correlation; dominant resemblance to low-threat category
		Armed Suspect	0.384	Weak similarity; limited behavioural match
		Trained Militant	0.633	Moderate alignment with militant-trained features
		High Value Target	0.666	Strongest in this category; noticeable resemblance to high-value target behaviour
Blue	T_3	Low Threat	0.618	Moderate resemblance to low-risk indicators
		Armed Suspect	0.494	Moderate-to-weak alignment with armed-suspect patterns
		Trained Militant	0.501	Moderate similarity to militant-trained signatures
		High Value Target	0.506	Weak-to-moderate resemblance to high-value features

The normalized behavior of correlation between the targets and the four kinds of threats is shown graphically in Figure 8. Four distinct colors black, yellow, pink, and red are used to depict the 3D bar graph's values, which are simultaneously normalized (scaled from 0 to 1). While the 3D depth and color strength provide a visual representation of high, medium, or low behavioral alignment between the threat classes, each bar has numerical values placed on it for easy reference. The normalization technique makes it possible to compare all categories on an equal footing, making the variations in behavioral similarity immediately apparent. The long red bar indicates that T_2 has the highest normalized score of 1.00 in the Low-Threat group, demonstrating how closely it resembles the markers of low-risk behavior. T_1 has the lowest normalized score (0.00, black), and T_3 has a reasonable value (0.48, yellow), indicating absolutely no link with low-threat behavior. On every target, the Armed-Suspect type has comparatively lower normalized correlations. In the yellow range, T_3 has the greatest value (0.42). T_1 has the lowest normalized score (0.05, pink) while T_2 is smaller (0.25, yellow), suggesting that there is no substantial resemblance. This color distribution shows a lack of uniformity with armed-suspect characteristics.

Trained-Militant T_1 has the strongest correlation (0.72, pink) among the Trained-Militant group, indicating that it has the most indicators of trained-militant behavior. T_3 shows a less significant resemblance (0.26, yellow), while T_2 has a moderate value (0.51, pink). The height and shading of the bars visually support T_1's supremacy in this category of threats. T_2 has the highest normalized similarity (0.57, pink) in the High-Value-Target category, while T_1 has an intermediate value (0.51, pink). The least aligned is T_3 (0.27, yellow). While T_3 is comparatively low, the concentration of T_1 and T_2 in the middle of values suggests a moderate resemblance to high value behavioral traits.

Generally speaking, each target's relative behavioral similarity to the designated target categories is effectively presented by the normalized 3D bar graph. Using distinct colors, bar heights, and numerical labels makes it simple to spot dominant patterns and weak associations in an effective way that makes using normalized correlation scaling to make decisions quick and easy to comprehend.

Table 12. Color interpretation for the normalized 3D Bar Graph

Color	**Normalized Range**	**Meaning in the Graph**	**Interpretation Role**
Black	0.00	Represents the minimum normalized correlation value	Indicates complete absence of behavioural resemblance with the given threat category
Yellow	0.25 - 0.48	Represents weak to moderate normalized correlation levels	Highlights mild behavioural similarity that does not strongly match the threat class
Pink	0.50 - 0.72	Represents moderate to strong normalized correlation	Indicates noticeable resemblance to the threat category, though not dominant
Red	1.00	Represents the maximum normalized value	Marks the strongest and most dominant behavioural alignment within the dataset

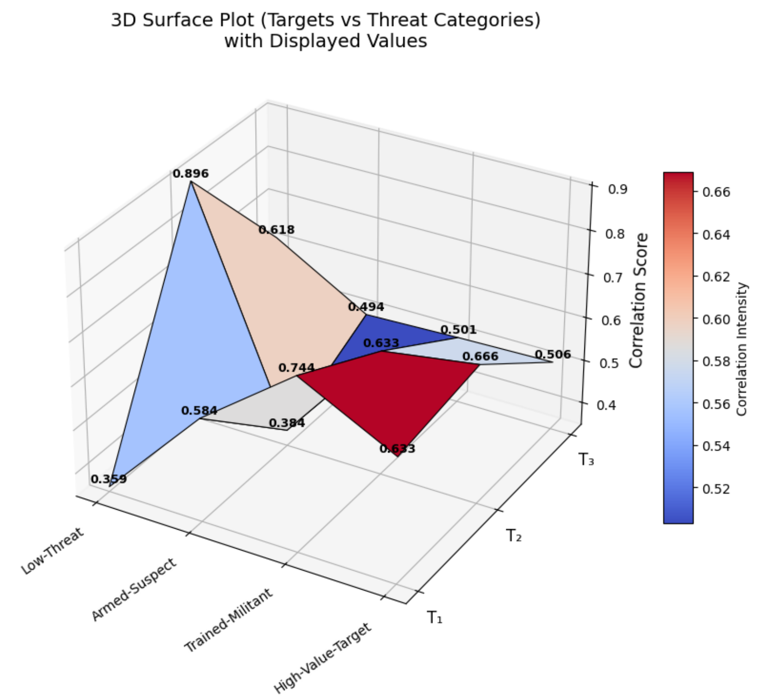

Figure 9

In order to produce a 3D surface plot, Figure 9 graphically depicts the correlation behavior of the suspected targets and the four threat categories. The surface mesh connects the correlation values of T_1, T_2, and T_3 across the threat classes, allowing the user to observe smooth transitions, peaks, and behavioral gradients between classes. The color map, which graphically depicts the degree of behavioral similarity, ranges from cool blue (lower correlation) to warm red (higher correlation). There is visual continuity on the plotted surface since the values are printed on the surface in numerical form, enabling explicit reference to each correlation score. The T_2 value, which rises to the greatest point of 0.896 and forms the largest peak at the left of the figure, is the maximum value in the Low-Threat category. T_1 has the lowest level (0.359), a downward slope that indicates a weak alignment with low-risk behavior, while T_3 has an intermediate value of high levels (0.618). At lower elevations, the Armed-Suspect region has a smoother surface, with T_1 having the highest score (0.584). T_2 is at the bottom (0.384), while T_3 has a respectable score (0.494). This is because this section's shape is rather flat and represents a consistently weak to moderate resemblance between targets and behavior. Once again, the Trained-Militant category produces surface peaks with T_1,0.744, resulting in a red-colored visual depiction. T_2 has a median score of 0.633, while T_3 has a lower plateau score of 0.501. The trend from T_1 to T_3 indicates a decrease in behavioral resemblance to militant-trained tendencies. The highest height in the High-Value-Target category is at T_2 (0.666), which creates a noticeable surface jump. T_1, which has an intermediate value (0.633), comes closely behind. T_3 (0.506) is the cluster's lowest point. In this instance, the less noticeable color shift results in a moderate-strong resemblance between T and T_2 and a weaker similarity between T_3. The 3D surface plot often provides an unbroken and intuitive depiction of the behavioral alignment between threat kinds and targets. Analysts may more easily identify the depths of low similarity and the heights of strong correlation with clarity and spatial integrity thanks to the rated color transitions, triangularine surface geometry, and clearly defined values in all.

Table 13. Color interpretation for the 3D Surface Plot

Color Shade	Normalized Range	Meaning in the Graph	Interpretation Role
Warm Red	≈0.65 - 0.90	Represents high-intensity correlation regions	Indicates strong behavioural resemblance to the threat category; appears at peaks such as T_1 Trained-Militant (0.744) and T_2 High-Value-Target (0.666)
Light Peach / Light Red	≈0.55 - 0.64	Shows moderate-to-high correlation	Highlights areas of noticeable but not dominant similarity, such as T_2 Trained-Militant (0.633)
Light Blue	≈0.45 - 0.54	Indicates moderate correlation regions	Suggests partial resemblance, such as T_3 Armed-Suspect (0.494) and T_3 Trained-Militant (0.501)
Cool Blue	≈0.35 - 0.44	Represents weak correlation zones	Marks low-resemblance patterns, including T_1 Low-Threat (0.359) and T_2 Armed-Suspect (0.384)

A 3D surface plot of the graphical representation of the normalized correlation behavior between the targets and the four threat categories is shown in Figure 10. The surface mesh, which enables direct comparison of the danger classes on a single scale, is the normalized (01 scaled) value of correlation of T_1, T_2, and T_3. The color map, which shows how strongly behavioral similarities occur, ranges from deep purple (lowest values) to teal and green to bright yellow (highest values). The numerical values are displayed atop each vertex to ensure that the normalized scores are easily identifiable without obscuring the surface's visual gradient. T_2, the bright yellow vertex with the highest normalized value of 1.000 in the Low-Threat category, shows the strongest correlation with indications of low-risk behavior. T_1 has the lowest normalized score (0.000, dark purple), indicating complete dissimilarity to low-threat behavior, whereas T_3 has a moderate value (0.482, green-teal area). The Armed-Suspect portion of the surface typically has weaker correlations. With a score of 0.419, T_3 does the best, followed by T_2 with a score of 0.251, and T_1, which is near zero (0.047). The low elevation and narrow color spectrum (purple-teal) suggest that all targets of this kind of threat share a limited resemblance. In the Trained-Militant category, T_1 has the highest normalized correlation (0.717), which is shown as a high, green-yellow portion of the surface. T_3 has a lower value (0.264), while T_2 has a moderate value (0.510). The decrease in behavioral resemblance to characteristics of militant training is indicated by the negative slope between T_1 and T_3. T_2 again has the highest normalized score (0.572, green yellow) in the High-Value-Target category, resulting in a distinct peak on the surface. T_3 is located in the lower mid-range (0.274), whereas T_1 has a moderate value (0.511). This suggests that while T_3 does not show considerable similarity to high-value target qualities in normalized scaling, T_2 and T_1 do. The target set's behavioral similarity is represented smoothly and continuously overall by the normalized 3D surface map. The analysts can quickly and easily assess the alignment of the threat categories in a state of normalized correlation by looking at the intensity of the dominant peaks, moderate plateaus, and low intensity areas thanks to the color gradient, related surface geometry, and value labels.

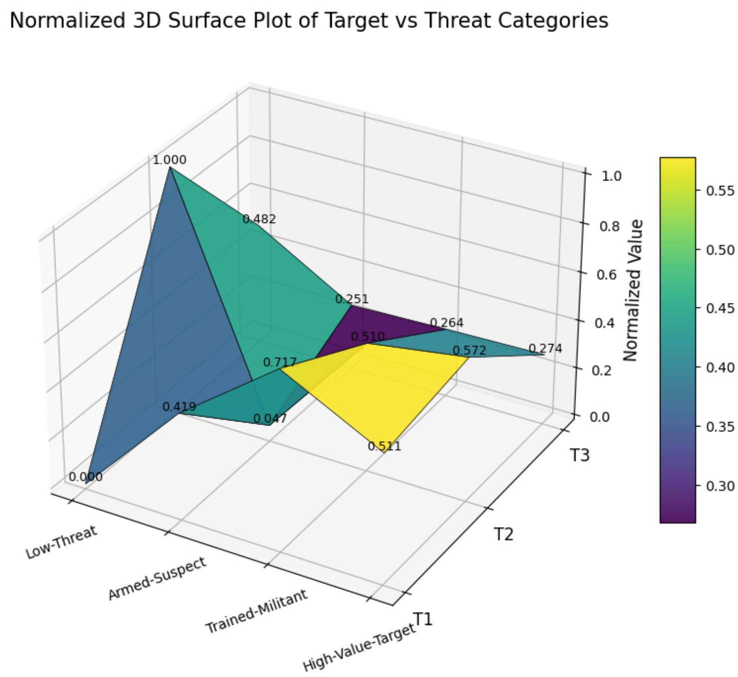

Figure 10

Table 14. Color interpretation for the 3D Surface Plot

Color Shade	**Normalized Range**	**Meaning in the Graph**	**Interpretation Role**
Bright Yellow	≈0.55 - 1.00	Represents the strongest normalized correlation values	Indicates dominant behavioural resemblance to the threat category; forms the highest peaks on the surface (e.g., T_2 Low-Threat = 1.000, T_2 High-Value-Target = 0.572)
Green / Teal	≈0.40 - 0.54	Shows moderate normalized correlation levels	Highlights meaningful but not dominant similarity (e.g., T_1 High-Value-Target = 0.511, T_2 Trained-Militant = 0.510)
Blue-Teal	≈0.25 - 0.39	Represents weak-to-moderate resemblance	Indicates partial behavioural alignment with reduced intensity (e.g., T_3 Trained-Militant = 0.264, T_2 Armed-Suspect = 0.251)
Deep Purple	≈0.00 - 0.24	Marks the lowest normalized correlation values	Indicates minimal or no behavioural resemblance; appears at the lowest surface points (e.g., T_1 Low-Threat = 0.000, T_1 Armed-Suspect = 0.047)

Using a 2D PCA projection of the K-Means clustering result, Figure 11 shows a graphical representation of the three targets' clustering behavior. In order to compare the three goals using the same dimensional scale, Principal Component Analysis (PC1 and PC2) produced a reduced dimensional space, which is shown by the scatter plot. The targets are labeled with the corresponding cluster label (C0 or C1), and the visual distance between the points shows the similarity structure that underlies the K-Means and two PCA techniques. Target T_2, which is situated in

Cluster C0 and has a positive PC1 and PC2 score, is plainly visible on the far right side of the plot. T_2's geographical isolation from the other two targets suggests that, in contrast to T_1 and T_3, it has a distinctive behavioral profile. Its high correlation coefficients in the Low-Threat and High-Value-Target categories, which make it an autonomous grouping in the reduced PCA space, are consistent with this separation. Targets T_1 and T_3 are located in Cluster C_1 and are predicted to be closer to one another along the PCA axes while having different relationships between threat categories. T_3 is in the lower-right corner with negative PC2 and positive PC1, whereas T_1 is on the left with moderately positive PC2 and negative PC1. As sampled on the major PCA components, their relative proximity implies that their joint threat-signature distribution is quite comparable. It is in line with the correlation values that they show in categories like High-Value-Target and Trained-Militant, which are very similar. Two groups can be clearly distinguished by the clustering effect:

Cluster C_0: a single person with unique behavior (T_2).

Cluster C_1: Two targets (T_1, T_3) in the PCA feature space with similar behavioral characteristics. The 2D PCA-based K-Means visualization offers a broadly interpretable picture of the targets' similarity patterns. The notion that T_2's behavioral profile is notably different from that of T_1 and T_3, whereas T_1 and T_3 are somewhat similar despite their differences in specific threat categories, is supported by the apparent distance between T_2 and the cluster that includes T_1 and T_3.

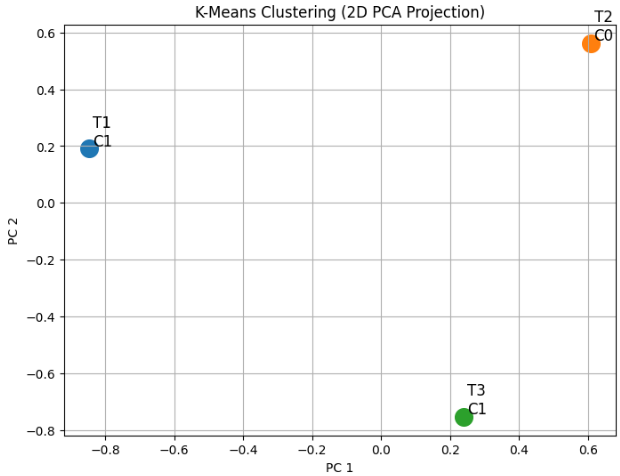

Figure 11

Table 15. Cluster assignments of targets (K-Means, 2D PCA Projection)

Target	**Cluster Label**	**PCA Position (PC1, PC2)**	**Interpretation**
T_1	C1	(Negative PC1, Moderate Positive PC2)	Assigned to Cluster 1 due to partial similarity with T_3; forms part of the compact behavioural grouping in PCA space.
T_2	C0	(High Positive PC1, High Positive PC2)	Sole member of Cluster 0; distinctly separated from T_1 and T_3, indicating a unique behavioural signature.
T_3	C1	(Positive PC1, Strong Negative PC2)	Assigned to Cluster 1 alongside T_1; relatively close to T_1 in reduced PCA space, showing overlapping behavioural characteristics.

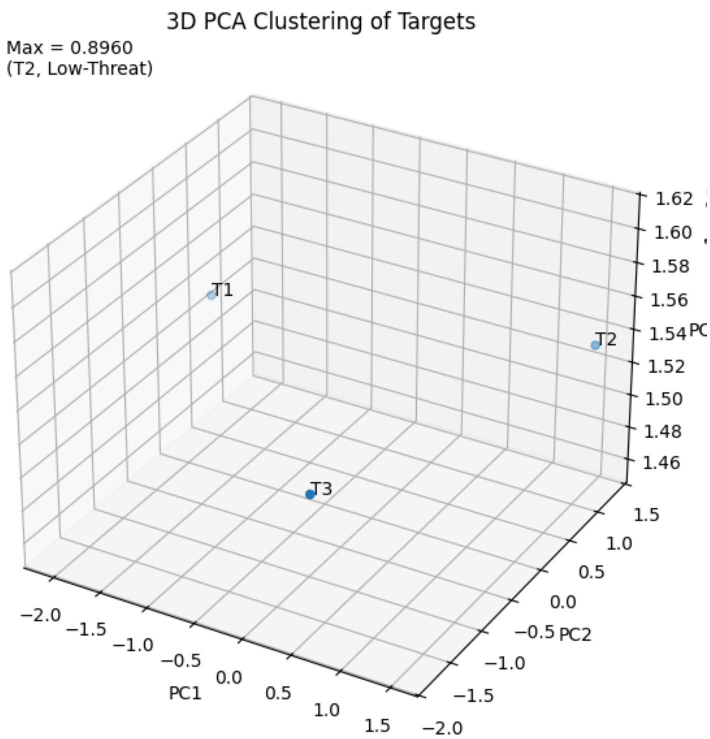

Figure 12

Figure 12 displays a 3D PCA clustering plot of a graphical depiction of the three potential targets in reduced feature space. In order to show the differences and similarities between the targets in three dimensions, the three main variables (PC1, PC2, and PC3) depict the current behavioral linkages in an orthogonal manner. Plotting the target points (T_1, T_2, and T_3) with matching PCA values reveals the Low-Threat category's greatest correlation value of 0.896 for T_2 as a contextual point in behavioral dominance. Target T_2 is easily seen in the upper-right corner of PCA space, with a reasonably high PC3 coordinate and positive PC1 and PC2 contributions.

The isolated position demonstrates that T_2's behavioral signature differs considerably from that of the other two targets. The separation, particularly its peak value with the Low-Threat group, is consistent with its high correlation trend in the prior instance. Target T_1 is located on the other side of the PCA space, however PC3 and PC1 have moderate and negative values. Divergent behavioral patterns are demonstrated by the fact that it is relatively far from T_2. The location of T_1 also shows that it has a reasonably significant correlation with categories such as Trained-Militant (0.744) and High-Value-Target (0.633), which sets it apart from the combined feature space of T_2 and T_3.

Target T_3 is positioned lower on the 3D PCA topography, with lower PC3, negative PC2, and moderately positive PC1. In comparison to T_1 and T_2, this coordinate frame suggests that T_3 has a weaker and more unclear behavioral pattern. The middle-weak similarities in the earlier correlation tables and surface plots are indicated by its clustering closer to T_1 than to T_2.

In general, the structural separation between targets can be effectively displayed using the 3D PCA scatter visualization:

T_1 is somewhat similar to T_3 but behaves differently,

T_2 is clearly a distinct object of behavior.

In PCA space, T_3 is at the bottom and has the least influence.

The 3D projection offers a condensed spatial representation of each target's variance in multidimensional behavioral space, complementing earlier findings of normalized surfaces, bar graphs, and clustering maps.

Table 16. PCA Coordinates of Targets (PC1, PC2, PC3)

Target	PC1	PC2	PC3	Interpretation
T_1	≈-1.5	≈0.2	≈1.55	Positioned on the negative PC1 side with moderate PC2 and high PC3, reflecting a behavioural profile distinct from T_2 but partially overlapping with T_3.
T_2	≈1.3	≈0.5	≈1.53	Located on the high positive PC1/PC2 region with elevated PC3, indicating a clearly distinct behavioural signature.
T_3	≈0.3	≈-0.7	≈1.47	Occupies lower PC2 and slightly positive PC1 with moderate PC3, reflecting weak-to-moderate similarity to T_1 and strong separation from T_2.

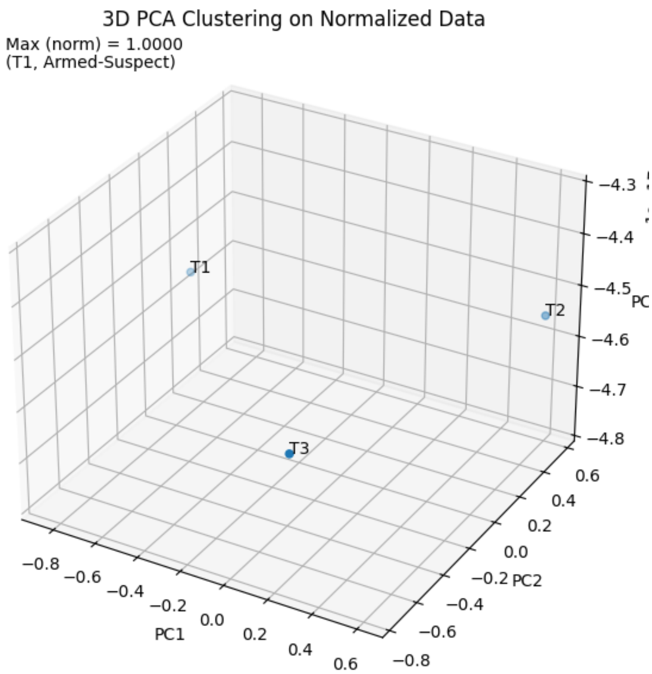

Figure 13

The three normalized principal components (PC1, PC2, and PC3) are shown in Figure 13, a graphical representation of the normalized and PCA transformed target distribution in the form of a 3D PCA clustering plot. This allows for the study of the behavioral structure of T_1, T_2, and T_3 in a scale-free space; normalization also transforms all correlation values within the range of 0 to 1; PCA is then applied, moving the spatial relationships between them, and each feature plays a proportionate role. The top-left annotation displays the highest normalized value (1.000), which is T_1 in the Armed-Suspect category. Target T_1 has a negative PC1, a slightly negative PC2, and a rather high PC3 value. It is situated in the upper-left corner of the PCA space. It indicates that T_1 is still in a modest distance from T_2 and T_3 while maintaining dominance in at least one of the standardized behavioral variables (armed-suspect similarities). This placement is consistent with earlier research showing that T_1 was moderately similar to the high-value-target categories and very comparable to the trained-militant categories. With positive PC1 and PC2 and intermediate range PC3, Target T_2 is situated on the right side of the PCA cube. Its relational profile has altered since normalization, as seen by the disconnection with T_1. Even though T_2 was once the strongest in the high-value and low-threat categories, normalization distributes influence across dimensions, causing T_2 to approach the center of the PCA space without necessarily losing much ground to T_1 and T_3. Target

T_3 has the lowest PC3 value of the three points, a moderately positive PC1, a negative PC2, and is in the bottom half of the PCA space. Given that T_3 does not exhibit a strong behavioral dominance in any one threat category, its position indicates that it exhibits modest-low normalized similarity across all threat types. The normalized 3D PCA space typically displays a triangular disentangling of the targets:
T_1 continues to be high on PC3, and this dominance is maintained in significant normalized dimensions.
T_2 exhibits balanced normalized behavior, occupying a middle-shifted region with moderate PCA contributions.
T_3, which is located in mid-PC1 and bottom PC3, is the least dominant in normalized dimensions.
As a result, the 3D PCA plot provides a consistent and visually understandable representation of how normalization changes the distance between behavioral inter-target behavioral distances. By removing scale-related distortions, the 3D plot enables more reliable target comparisons.

Table 17. Normalized PCA Coordinates of Targets (PC1, PC2, PC3)

Target	**PC1 (Normalized)**	**PC2 (Normalized)**	**PC3 (Normalized)**	**Interpretation**
T_1	≈-0.75	≈-0.10	≈-4.40	Positioned on the negative PC1 side with moderate PC2 and high PC3, reflecting a behavioural profile distinct from T_2 but partially overlapping with T_3.
T_2	≈0.55	≈0.45	≈-4.52	Located on the high positive PC1/PC2 region with elevated PC3, indicating a clearly distinct behavioural signature.
T_3	≈0.25	≈-0.55	≈ -4.75	Occupies lower PC2 and slightly positive PC1 with moderate PC3, reflecting weak-to-moderate similarity to T_1 and strong separation from T_2.

A set of cubic spline-smoothed functional curves illustrating the behavior of each threat category on the three targets (T_1, T_2, and T_3) are displayed in Figure 14. In contrast to discrete point plots, spline interpolation creates smooth, continuous curves that more clearly highlight underlying patterns. Every category of threat is represented by a curve, and the exact numerical values are drawn at the original data points so that one may immediately refer to the curve and still benefit from the spline smoothing's visual effect. Between T_1 and T_3, the Low-Threat curve (blue) shows an increasing tendency. The value rises in the same direction from T_1's 0.359 to T_2's 0.584 and T_3's 0.744. This linear trend indicates that behavior and low-threat qualities are becoming more similar between T_1 and T_3, with T_3 having the most similarity. An alternative U-shaped curve is the Armed-Suspect curve (orange). With a value of 0.584, T_1 would have the greatest value, followed by T_2 with a lower value of 0.384 and T_3 with a higher value of 0.633. The spline between T_1 and T_2 has a downward dip because this pattern shows that T_1 and T_3 are more or less comparable to armed-suspect indicators, while T_2 is the least similar. From T_1 to T_3, the Trained-Militant curve (green) exhibits a consistent declining trend.
At T_1, the curve starts to slope higher with a value of 0.744; at T_2 and T_3, it drops to 0.633 and 0.506, respectively. T_1 and T_3 had the greatest and least similarities to trained-militant behavior, respectively, according to this negative slope. The rising and downward slopes of the red High-Value-Target curve are smooth. It starts at 0.633 with T_1, increases little to 0.666 with T_2, and then decreases once more to 0.633 with T_3. With T_2 having the strongest link with high-value target signatures, albeit marginally higher than both of the other targets, the arc is nearly symmetrical, demonstrating a balance in the targets' similarities. Overall, a visually consistent representation of the behavioral alignment trend over targets has been provided by the spline-smoothed curves. The relationship between each type of danger and T_1, T_2, and T_3 is explained by their various shapes, which include rising, declining, U-shaped, and peaked. The labels of the plotted values provide numerical transparency, while the data's underlying structural patterns can be found using the smooth curves.

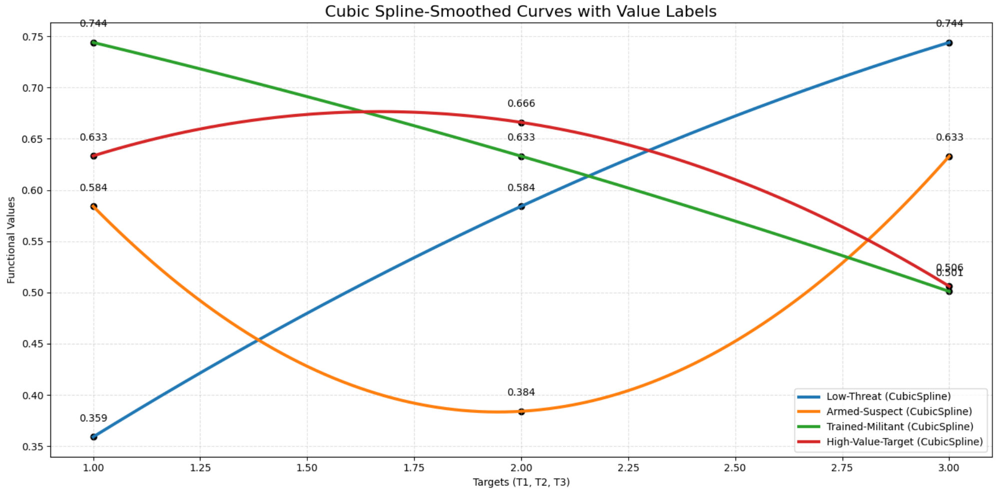

Figure 14

Table 18. Color Interpretation for Cubic Spline-Smoothed Functional Curves

Color	**Threat Category**	**Meaning in the Curve**	**Interpretation Role**
Blue	Low-Threat	Represents the functional behaviour of Low-Threat similarities across T_1-T_3	Indicates a steadily increasing resemblance, strongest for T_3 and weakest for T_1
Orange	Armed-Suspect	Shows the spline-smoothed values for Armed-Suspect correlation	Highlights a U-shaped pattern, with high similarity at T_1 and T_3 but a pronounced dip at T_2
Green	Trained-Militant	Depicts the decreasing functional trend of trained-militant resemblance	Indicates strongest similarity at T_1, moderate at T_2, and weakest at T_3
Red	High-Value-Target	Represents the smoothed pattern of high-value target alignment	Shows a slight rise and fall pattern, peaking at T_2 and symmetric around T_1 and T_3

Following min/max normalization, Figure 15 displays a set of normalized cubic spline-smoothed curves that illustrate the behavior of each threat category over the three targets T_1, T_2, and T_3. The displayed normalized numbers preserve numerical clarity while the smoothing effect highlights each category's general direction. The four levels of threat are represented by the curves, which are colored yellow, red, green, and black. Numerical labels are printed at each target point to make it simple to relate to the values. With an initial value of 0.401 and a maximum value of 1.000 at T_2, the Low-Threat curve (yellow) exhibits a high inclination between T_1 and T_2. At T_3, which has a value of 0.690, the curve similarly begins to decline at this point. The normalized similarity to low-threat traits is smallest at T_1, strongest at T_2, and relatively high at T_3, according to this convex, arch-shaped behavior. When it comes to low-threat resemblance, the fact that the largest value is at T_2 shows that it is the predominate value even on the normalized scale. The smooth U-shaped evolution of the Armed-Suspect curve (red). It starts at 0.652 with T_1, drops to 0.429 with T_2, and then rises to 0.655 with T_3. Similar to earlier raw-value results, this form shows that T_1 and T_3 are more strongly associated with armed-suspect characteristics than T_2, which is the least so in this group.
The trend in the Trained-Militant curve (green) increases consistently from T_1 and T_2, moving from 0.707 to 0.743 before slightly declining to 0.651 at T_3. T_2 has the highest normalized similarity with militant-trained behavior, while T_3 has the lowest, however the differences are not significant due to normalization compression, according

to the steady up and down trend. Between T_1 (0.830) and T_2 (0.706), the High-Value-Target curve (black) slopes slightly downward before falling to 0.651 at T_3. T_1 has the largest normalized similarity with the traits of high-value targets, as demonstrated by the fact that T_2 and T_3 have somewhat lower similarity. Overall, when scaled, the normalized spline-curves provide a visual comparison of the threat-category similarity distribution of targets. Strong and weak behavioral inclinations are revealed by the continuous curves, distinct color coding, and numbered values, which also make it possible to provide an accurate and intuitive interpretation of the threat alignment under typical correlation conditions.

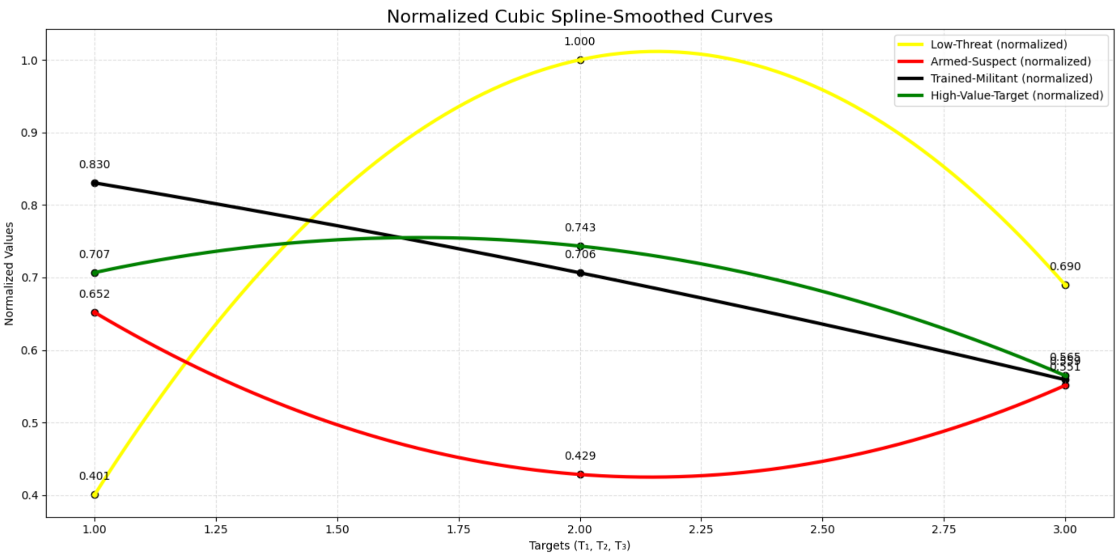

Figure 15

Table 19. Normalized spline values for threat categories Across Targets

Target	**Low-Threat (Yellow)**	**Armed-Suspect (Red)**	**Trained-Militant (Green)**	**High-Value-Target (Black)**
T_1	0.401	0.652	0.707	0.830
T_2	1.000	0.429	0.743	0.706
T_3	0.690	0.655	0.651	0.651

8. Aspect-method interpretation of neutrosophic correlation behaviour of target-level threat assessment.

The goal of this synthesis is to integrate the neutrosophic soft correlation system's methodological and behavioral viewpoints. Aspect-wise, the correlation process's outcomes are useful in assigning each target to a threat category that best reflects it; T_1 is a militant-oriented profile, whereas T_2 and T_3 are less dangerous and behave similarly. The weighted neutrosophic correlation operator consistently replicates threat patterns in heatmaps, PCA plots, clustering structures, and surface-based plots, demonstrating its high-grade computational reliability. When taken as a whole, aspect and technique views confirm that the proposed structure is reliable, comprehensible, and effective in converting the ambiguous surveillance signals into a logical and data-driven threat assessment.

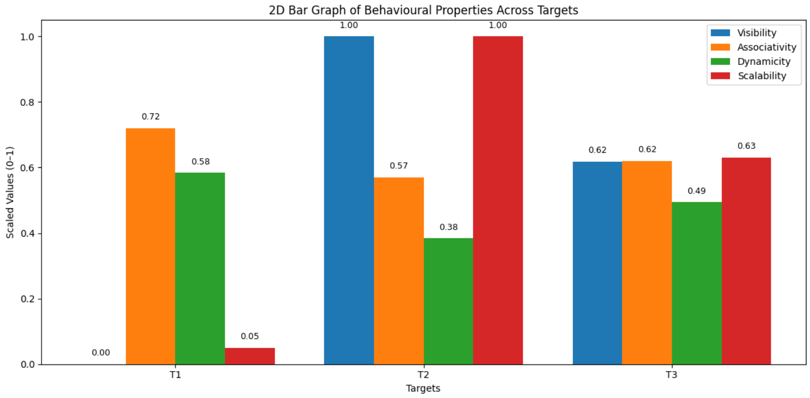

Figure 16

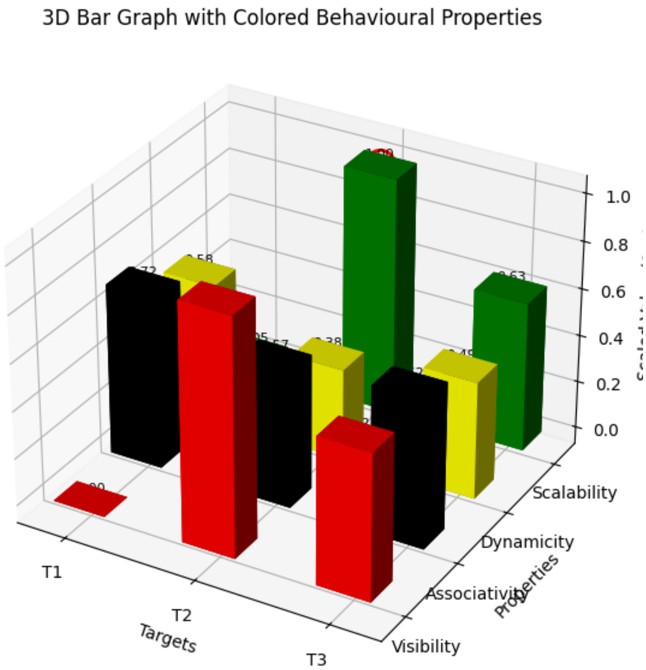

Figure 17

8.1. Aspect-based Analysis

Threat Identification Accuracy and Target-Profile Similarity and Distinction are two important factors that can be used to analyze the correlation output. These factors show how well the neutrosophic soft correlation framework distinguishes between different risk levels when there is uncertainty.

Threat Identification Accuracy: The correlation table indicates that the approach's primary effect is to assign any target to the most likely threat category with the highest neutrosophic soft correlation score. T_1 shows the highest alignments with the Trained-Militant aspect (0.7440), which suggests the behavioral indicators of coordinated or tactical hostile action. T_2 shows the highest correlation with the Low-Threat component (0.896), suggesting that the overall behavior pattern is closer to the low-risk indicators when there are intermittent cues. In contrast to strong high threat signs, T_3 exhibits a nearly identical but marginally greater correlation with the low threat aspect

(0.618), which denotes an ambiguous and ambivalent behavioral style with modest amounts of suspicion indicators. This demonstrates how the technique may convert ambiguous and contradictory surveillance material into a clear, quantitatively based assessment of each target's threat.

Target-Profile Similarity and Distinction: The distribution of correlation between the four threat categories reveals the underlying profile structure. The correlation patterns of T_2 and T_3 are similar; they both show moderate to low correspondence among the other threat classes and a relatively strong affinity with Low-Threat cues. It indicates that the uncertainty qualities are overlapping and that the two targets are members of a behaviorally dependent subgroup. On the other hand, T_1 exhibits a markedly different pattern, with a substantial correlation between the traits of High-Value-Target and Trained-Militant. It is distinct and possibly a high-risk organization due to its comparatively lesser correlation with Low-Threat behavior. The more exacting clustering, PCA costumes, and surface-plot visualizations that consistently separate T_1 from the T_2 T_3 grouping and validate aspect-based behavioral separation seen in the correlation matrix later corroborate this observation.

8.2. Method-based Analysis

The computational behavior of the neutrosophic soft correlation measure and the structural consistency shown throughout the generated visual analytics are the two main components of the system's methodological meaning. When combined, these components show how the recommended method converts unclear reconnaissance indicators into reliable and measurable threat evaluations.

Operational Performance of the Correlation Measure: The correct computation of the neutrosophic soft correlation coefficients, which assign each target to the most representative threat category, is the first methodological implication. The method employs the weighted correlation operator $C(\mathcal{A}, \mathcal{B})$ to encompass the composite behavioral alignment while combining the aspects of truth, indeterminacy, and falsity. The obtained coefficients successfully indicate the dominant behavioral type of each target: T_1 is classified as Trained-Militant, T_2 as Low-Threat, and T_3 as fairly low-risk. The fact that the provided approach can effectively handle incomplete, noisy, and conflict-based intelligence signals and transform them into a form of interpretable threat-classification output is a hint that it is operating as intended.

Structural Uniformity Among Analytical Methods: The degree to which the correlation patterns are preserved using additional visualization and clustering techniques gives rise to the second methodological dimension. The use of Heatmaps, PCA projections,3D surfaces plots, spline-smoothed curves, and cluster mappings all give the same relative similarities and separations between T_1, T_2 andT_3. As an example, T_1 is clearly separate over PCA clusters and surface gradients, which confirms the initial correlation-based separation. Meanwhile, T_2andT_3 are situated quite closely in the visual representations, demonstrating their closeness as revealed by the correlation patterns. The fact that structural behaviour is conserved over various methodological levels in the suggested framework indicates the stability of the offered framework and proves that the measure of correlation is not only mathematically consistent but also stable visually and analytically.

9. Comparative behavioural properties with numerical indicators

Visibility: The degree to which a system's internal behavior, internal structure, or internal decision-making patterns may be observed, deciphered, or followed is known as its visibility. In a nutshell, it refers to how simple it is for us to see what is going on within the system. High visibility in analytical or computational models ensures easier interpretation, traceability, and transparency of the outputs produced, while low visibility turns the system into a "black box" where judgments are difficult to understand or defend. The attribute is crucial because it makes the system understandable, makes it easier to validate and debug computational processes, and is shown to be especially crucial in delicate applications like threat analysis, diagnostic reasoning, or security-critical decision-making.

Associativity: The degree to which the components of a system are connected, linked, or related to one another is referred to as associativity. To put it simply, it is a gauge of how much different things belong. Associativity evaluates a number of factors, including the evaluation of pattern consistency in analytical structures, the identification of clusters or similarities or behavioral predispositions, and the strength of links between inputs

and outputs. This trait is crucial since it is fundamental to correlation-based systems and immediately helps with accurate categorization, prediction, and decision-making.
Dynamicity: A system's ability to adapt to changes brought about by its surroundings, the data it receives, changes in its behavior, or changes in the degree of uncertainty is known as its dynamicity. In practical terms, it is the reaction to systemic changes in a way that would be satisfying. Dynamic is helpful in the computational model's real-time updates, responds well to variations in input signals, and becomes flexible when faced with ambiguities or insufficient data. This feature is crucial since it will enable real-time danger identification and maintain system stability in the face of noise, contradictory indications, or continuously shifting patterns.
Scalability: The ability of a system to function up to a higher and more complex workload is known as scalability. To put it simply, can it handle bigger, more challenging, and data-intensive tasks without failing? This is due to the fact that in an analytical system, the amount of characteristics that indicate a threat category or the addition of additional targets and features would not affect the model's efficiency. It can process data quickly on a wide scale and is neither computationally unstable nor inaccurate. This is crucial since, in practice, operational systems should be dependable as datasets grow so that the framework won't be jeopardized and can instead function, be deployed, and operate in high-volume or real-time scenarios. This table includes the numerical values of Figs and depicts your entire correlation ecology in four system-level behavioral properties: visibility, associativity, dynamicity, and scalability. 2-15 (normalized values, Pearson values, and raw scores). 20: Table for target-threat correlation behavioral property analysis.

Table 20. Factor-Based Comparison of Analytical Techniques

Property	**Definition (Context of Threat Correlation)**	**How It Appears in Figs. 1-14**	**Numerical Indicators (Extracted From Your Results)**	**Interpretation**
Visibility	The clarity with which a target's behavioural signature emerges across threat classes; measured by how distinct or discernible its correlations are.	Strong color separations in Heatmaps (Figures 2, 3, 4) and dominant peaks in 2D/3D bar graphs (Figs. 5-6).	**High visibility:** T_2 Low-Threat = 0.896 (Figure 2), Pearson = 1.20 (Figure 4), Normalized = 1.00 (Figure 4). **Low visibility:** T_1 Low-Threat = 0.359, Pearson = -1.37, Norm = 0.00.	T_2 is the most visible, with consistently strong peaks; T_1 shows low visibility for low-threat traits.
Associativity	Degree of similarity between a target and threat category; measured through correlation strength, Pearson direction, and normalized closeness.	Highlighted via circled maxima in Heatmaps, bar graphs, and spline curves (Figs. 2-15).	**Strong associations:** T_1 Trained-Militant: 0.744 (raw), 1.01 (Pearson), 0.72 (norm). T_2-HVT: 0.666 (raw), 0.10 (Pearson), 0.57 (norm).	T_1 associates strongly with militant behaviour; T_2 with low-threat & high-value categories.
Dynamicity	How much the target's behavioural resemblance changes across categories; measured via fluctuations in raw vs normalized values and spline curvature.	Captured by rising/falling spline curves (Figures 14-15), change of color gradients in Heatmaps.	**High dynamicity:** Armed-Suspect spline: T_1=0.584 $\rightarrow$ T_2=0.384 $\rightarrow$ T_3=0.494 (U-shape). **Low dynamicity:** HVT spline: 0.633 $\rightarrow$ 0.666 $\rightarrow$ 0.633 (near flat).	Armed-Suspect is the most dynamic category; HVT is the most stable.
Scalability	Stability of behavioural patterns under normalization, PCA reduction, and dimensional scaling.	Reflected in PCA positions (Figures 11-13) and normalized 3D surfaces (Figures. 8-10).	**Stable under scaling:** T_2 remains dominant for Low-Threat even after full normalization: Raw=0.896 $\rightarrow$ Norm=1.00 $\rightarrow$ PCA peak (PC1$\approx$1.3). **Unstable under scaling:** T_1 Armed-Suspect: 0.584 $\rightarrow$ 0.05 (normalized) $\rightarrow$ PCA shift to negative PC1.	T_2 is highly scalable (keeps dominance), while T_1's relationships weaken under scaling.

10. Conclusion

Using Pythagorean Neutrosophic Sets (PNS) and the correlation structure, the study creates a theoretical and practical framework for analyzing and understanding ambiguous behavioral data. A mathematically consistent handling of incomplete, conflicting, and ambiguous data is ensured by the PNS axioms, which are defined by membership, indeterminacy, and non-membership terms provided by Pythagorean limitations. Complement, union, intersection, and squared-component correlation measures are the computational tools used to evaluate the similarity between neutrosophic entities. It is a correlation operator that is symmetric and bounded between zero and one, making it a trustworthy quantitative technique for determining the strength of the relationship between two neutrosophic profiles. Based on this, the proposed neutrosophic soft correlation measure is applied to a real-world threat identification scenario in which four behavioral indications have been linked to four potential threat categories and three potential targets are under consideration. The approach creates a final correlation table that clearly illustrates each target's behavioral patterns by combining the target-behavior and behavior-threat relationship matrices. The results show that T_1 is the most suspicious object due to its preponderant similarity to the Trained-Militant category (0.744), whereas T_2 is closely related with the Low-Threat category (0.896). T_3 is found to have a moderate, balanced connection with every class, suggesting a low-signage or uncertain profile. These findings show that the proposed method is effective in converting dispersed, noisy, and indeterminate surveillance indications, such as thermal images, motion patterns, communication bursts, or handling weapon patterns, into comprehensible threat-level forecasts. The framework's interpretation of hybrid aspects and method further enhances the framework's stability and credibility. In terms of aspect, the correlation signatures consistently distinguish between high and low-risk behavioral groups, separating T_1 as an exclusive militant-aligned profile and combining T_2-T_3 into behaviorally similar low-risk entities. In terms of method, the weighted correlation operator also exhibits high computational robustness and structural consistency in heatmaps, PCA embeddings, spline curves, surface plots, and clustering geometries. These patterns' consistent persistence throughout the many levels of analysis demonstrates the framework's dependability, interpretability, and operational suitability. Overall, the study demonstrates that the neutrosophic soft correlation approach provides a reliable, scalable, and comprehensible threat assessment mechanism in ambiguous circumstances. The framework enables real-time decision-making in scenarios where behavior data is ambiguous, incomplete, or dynamically changing while maintaining mathematical rigor and practical interpretability.

11. Limitations and Future Work

The proposed neutrosophic correlation framework has several limitations that can be used to improve it, despite the fact that it is quite interpretable and stable in its analysis capabilities.

11.1. Limitations

First off, just three targets and four categories of threats are covered by the behavioral data used in the study, which restricts the framework's ability to be expanded to larger and more varied operational situations. According to this model, all targets exhibit the same neutrosophic patterns in behavioral indicators. However, actual surveillance evidence may exhibit greater variability, quicker temporal changes, or multi-modal inconsistencies that the current model is unable to effectively capture. Furthermore, despite its strength, the correlation measure is based on squared neutrosophic components, which may overemphasize strong behavioral signs and underrepresent weak but significant signals. Additionally, the paradigm operates under the assumption of snapshot behavior; it does not specifically address the concepts of temporal change, continuous data flow, or adversary deception tactics, all of which are prevalent in real-world security issues.

11.2. Future Work

Larger, real-world datasets of different behavioral fingerprints of sensor networks, drone imagery, communication data, and multi-spectral data can be incorporated into future research to further expand the system. In order to follow changes in behavior over time and offer a real-time threat tracking system, the framework needs additionally include dynamic updating techniques or temporal neutrosophic modeling. Enhancing the correlation operator to enable adaptive weighting, cross-feature interactions, or machine-learning assisted estimate could lead to further increases in sensitivity to weak or emergent danger indicators. The next potential approach is to create a multi-layered hybrid threat-detection pipeline by combining the output of the neutrosophic correlations with deep learning embeddings, clustering techniques, or Bayesian filters. Finally, the system can be implemented in command and control scenarios where transparency, traceability, and rapid interpretability are required thanks to the explainable AI modules and decision-support dashboards. Larger, real-world datasets of behavior patterns obtained from sensor networks, drone photography, communication signals, and multi-spectral data can be included into the suggested framework to improve its robustness and generalizability. It can be further expanded with temporal neutrosophic modeling and dynamic updating techniques to provide continuous monitoring and real-time threat assessment that takes into account changing behavioral patterns over time. Additionally, adaptive weighting techniques, cross-feature interaction analysis, and machine learning-based parameter estimation can be used to improve the sensitivity of the suggested correlation operator to weak, uncertain, and emergent danger indicators. Building a multi-layered hybrid threat-detection system with neutrosophic correlation measurements, clustering, and Bayesian filters for enhanced predictive power has a lot of potential. In order to ensure transparency, traceability, and prompt interpretation of crucial decisions, the framework may also be modified for command-and-control operations employing explainable AI and interactive dashboards for decision support. Future studies may investigate the new class of Floquet-engineered point-gapped topological superconductors [36] and non-Hermitian second-order topological phases in photonic kagome crystals [37] with ”bipolar” skin effects, in addition to intelligent danger detection. Future generation photonic and defensive technologies, robust communication systems, quantum sensing, and innovative and powerful signal processing might all be produced by integrating these cutting-edge ideas into neutrosophic decision making and threat analysis.

Acknowledgement

The authors also extend their appreciation to the Deanship of Scientific Research at Northern Border University, Arar, KSA, for funding this research work through the project number NBU-FFR-2026-2230-07.
Authors’ Contributions: All the authors contributed significantly in writing this article. The authors read and approved the final manuscript.
Competing Interests: The authors declare that they have no competing interests.

REFERENCES

1. L. A. Zadeh, *Fuzzy sets*, Information and Control, vol. 8, no. 3, pp. 338–353, 1965.
2. I. Turksen, *Interval valued fuzzy sets based on normal forms*, Fuzzy Sets and Systems, vol. 20, no. 2, pp. 191–210, 1986.
3. K. Atanassov, *Intuitionistic fuzzy sets*, Fuzzy Sets and Systems, vol. 20, no. 1, pp. 87–96, 1986.
4. K. Atanassov and G. Gargov, *Interval valued intuitionistic fuzzy sets*, Fuzzy Sets and Systems, vol. 31, no. 3, pp. 343–349, 1989.
5. X. C. Liu, *Entropy, distance measure and similarity measure of fuzzy sets and their relations*, Fuzzy Sets and Systems, vol. 52, no. 3, pp. 305–318, 1992.
6. W. Pedrycz and F. Gomide, *An Introduction to Fuzzy Sets: Analysis and Design*, MIT Press, Cambridge, MA, USA, 1998.
7. F. Smarandache, *A Unifying Field in Logics: Neutrosophy. Neutrosophic Probability, Set and Logic*, American Research Press, Rehoboth, NM, USA, 1999.
8. E. P. Klement, R. Mesiar, and E. Pap, *Triangular Norms*, Springer, Dordrecht, The Netherlands, 2000.
9. H.-J. Zimmermann, *Fuzzy Set Theory—and Its Applications*, 4th ed., Springer, Berlin, Germany, 2001.
10. D. F. Li and C. Cheng, *New similarity measures of intuitionistic fuzzy sets and application to pattern recognitions*, Pattern Recognition Letters, vol. 23, no. 1–3, pp. 221–225, 2002.
11. F. Smarandache, *Neutrosophic set: A generalization of the intuitionistic fuzzy set*, International Journal of Pure and Applied Mathematics, vol. 24, no. 3, pp. 287–297, 2005.
12. H. Wang, F. Smarandache, Y. Q. Zhang, and R. Sunderraman, *Interval Neutrosophic Sets and Logic: Theory and Applications in Computing*, Hexis, Phoenix, AZ, USA, 2005.
13. W. L. Hung and M. S. Yang, *Similarity measures of intuitionistic fuzzy sets based on L_p metric*, International Journal of Approximate Reasoning, vol. 46, no. 1, pp. 120–136, 2007.

14. H. D. Cheng and Y. Guo, *A new neutrosophic approach to image thresholding*, New Mathematics and Natural Computation, vol. 4, no. 3, pp. 291–308, 2008.
15. Y. Guo and H. D. Cheng, *New neutrosophic approach to image segmentation*, Pattern Recognition, vol. 42, no. 5, pp. 587–595, 2009.
16. J. Ye, *Multicriteria fuzzy decision-making method based on a novel accuracy function under interval-valued intuitionistic fuzzy environment*, Expert Systems with Applications, vol. 36, no. 3, pp. 6899–6902, 2009.
17. J. Ye, *Multicriteria group decision-making method using the distance-based similarity measures between intuitionistic trapezoidal fuzzy numbers*, International Journal of General Systems, vol. 41, no. 7, pp. 729–739, 2012.
18. R. R. Yager and A. M. Abbasov, *Pythagorean membership grades, complex numbers, and decision making*, International Journal of Intelligent Systems, vol. 28, no. 5, pp. 436–452, 2013.
19. R. R. Yager, *Pythagorean membership grades in multicriteria decision making*, IEEE Transactions on Fuzzy Systems, vol. 22, no. 4, pp. 958–965, 2014.
20. H. Wang, F. Smarandache, Y. Zhang, and R. Sunderraman, *Single-valued neutrosophic sets*, Review, vol. 17, pp. 10–14, 2010.
21. P. Liu and P. Wang, *Multiple-attribute decision-making based on Archimedean Bonferroni operators of q-rung orthopair fuzzy numbers*, IEEE Transactions on Fuzzy Systems, vol. 27, no. 5, pp. 834–848, 2019.
22. M. Abdel-Basset, M. Saleh, A. Gamal, and F. Smarandache, *An approach of TOPSIS technique for developing supplier selection with group decision making under type-2 neutrosophic number*, Soft Computing, vol. 23, no. 24, pp. 13257–13276, 2019.
23. M. Abualhomos et al., *Unified framework for type-n extensions of fuzzy, neutrosophic, and plithogenic offsets: Definitions and interconnections*, Journal of Fuzzy Extensions and Applications, vol. 6, no. 4, pp. 689–726, 2025.
24. A. Ahmad et al., *A study of some neutrosophic derivatives problems based on Newton's BDF and CDF numerical methods*, International Journal of Neutrosophic Science, pp. 1–8, 2025.
25. H. Edduweh et al., *On the weak fuzzy complex differential equations and some types of the 1st order 1st degree WFC-ODEs*, International Journal of Neutrosophic Science, pp. 450–468, 2025.
26. M. Abualhomos et al., *An effective algorithm for solving weak fuzzy complex Diophantine equations in two variables*, International Journal of Neutrosophic Science, 2024.
27. H. Zureigat et al., *Numerical solution of fuzzy heat equation with complex Dirichlet conditions*, International Journal of Fuzzy Information Systems, vol. 23, pp. 11–19, 2023.
28. R. Hatamleh, *On the Form of Correlation Function for a Class of Nonstationary Field with a Zero Spectrum*, Rocky Mountain Journal of Mathematics, vol. 33, no. 1, pp. 159–173, 2003.
29. R. Hatamleh and V. A. Zolotarev, *On Two-Dimensional Model Representations of One Class of Commuting Operators*, Ukrainian Mathematical Journal, vol. 66, no. 1, pp. 122–144, 2014.
30. R. Hatamleh and V. A. Zolotarev, *On Model Representations of Non-Selfadjoint Operators with Infinitely Dimensional Imaginary Component*, Journal of Mathematical Physics, Analysis, Geometry, vol. 11, no. 2, pp. 174–186, 2015.
31. R. Hatamleh and V. A. Zolotarev, *Triangular Models of Commutative Systems of Linear Operators Close to Unitary Operators*, Ukrainian Mathematical Journal, vol. 68, no. 5, pp. 791–811, 2016.
32. A. S. Heilat, H. Zureigat, R. Hatamleh, and B. Batiha, *New Spline Method for Solving Linear Two-Point Boundary Value Problems*, European Journal of Pure and Applied Mathematics, vol. 14, no. 4, pp. 1283–1294, 2021.
33. A. Qazza, I. Bendib, R. Hatamleh, R. Saadeh, and A. Ouannas, *Dynamics of the Gierer–Meinhardt Reaction–Diffusion System: Insights into Finite-Time Stability and Control Strategies*, Partial Differential Equations in Applied Mathematics, vol. 14, Art. 101142, 2025.
34. T. Qawasmeh, A. Qazza, R. Hatamleh, M. W. Alomari, and R. Saadeh, *Further Accurate Numerical Radius Inequalities*, Axioms, vol. 12, no. 8, Art. 801, 2023.
35. A. Shihadeh, K. A. M. Matarneh, R. Hatamleh, M. O. Al-Qadri, and A. Al-Husban, *On the Two-Fold Fuzzy n-Refined Neutrosophic Rings for $2 \leq n \leq 3$*, Neutrosophic Sets and Systems, vol. 68, pp. 8–25, 2024.
36. X. Ji, H. Geng, N. Akhtar, and X. Yang, *Floquet Engineering of Point-Gapped Topological Superconductors*, Physical Review B, vol. 111, Art. 195419, 2025.
37. X. Yang, Y. Feng, A. Wahab, and H. Geng, *Non-Hermitian Second-Order Topological Phases and Bipolar Skin Effect in Photonic Kagome Crystals*, Physical Review A, vol. 113, Art. 023506, 2026.